Neurons in the medial prefrontal cortex are involved in spatial tuning and signaling upcoming choice independently from hippocampal sharp-wave ripples.

Hanna den Bakker[1,2,*], Fabian Kloosterman[1,2]

1 Neuro-Electronics Research Flanders, Leuven, Belgium

2 Brain & Cognition, KU Leuven, Leuven, Belgium

* Corresponding author: hanna.denbakker@kuleuven.be

ABSTRACT

The hippocampus is known to encode spatial information and reactivate experienced trajectories during sharp-wave ripple events. These events are thought to be key time-points at which information about learned trajectories is transferred to the neocortex for long-term storage. It is unclear, however, how this information may be transferred and integrated in downstream cortical regions. In this study, we performed high-density probe recordings across the full depth of the medial prefrontal cortex and in the hippocampus simultaneously in rats while they were performing a task of spatial navigation. We find that neurons in the medial prefrontal cortex encode spatial information and reliably predict upcoming choice on a maze, and we find that a subset of neurons in the mPFC is modulated by hippocampal sharp-wave ripples. However, sharp-wave ripple modulation does not appear to be the main driving factor in predicting upcoming choice. This indicates that the integration of spatial information requires the collaboration of different specialized populations of neurons.

KEYWORDS: hippocampus, prefrontal cortex, spatial learning, replay

Number of figures: 6
Number of tables: 0
Number of supplementary figures: 4
Number of supplementary tables: 1

Abstract: 158 words
Introduction: 777 words
Results: 3658 words
Discussion: 1291 words
Methods: 3891 words

INTRODUCTION

The hippocampus is known to be important for spatial navigation. This is largely attributed to the spatially specific firing patterns of place cells, which fire sequentially as animals navigate through an environment in the timeframe of theta frequency (~8Hz) oscillations. These sequential firing patterns are often repeated or ''replayed'' during short high frequency oscillations called sharp-wave ripples (SWRs) while the animal is in a state of behavioral immobility or sleep. The function of these replay patterns is still somewhat under debate, but during awake immobility periods they have been proposed to either predict immediate future behavior[1–5], or reflect specific past experience[6], and adapt to reward[7,8] and task demand[9], while during sleep, they are thought to be important for memory consolidation[10].

A running hypothesis is that the hippocampus transfers information to neocortical areas during these SWR events and this is thought to be a crucial mechanism to facilitate spatial learning[11]. Congruently, it has been shown that a subset of neurons in the medial prefrontal cortex shows modulated firing patterns following SWRs in the hippocampus, where some neurons show an increase and others a decrease of firing rate, both in a 200 millisecond window following SWR onset[12,13]. Disrupting this window of activity in the mPFC slowed the acquisition of a spatial rule reversal[14].

The mPFC can be divided into three regions: the anterior cingulate cortex (ACC), the prelimbic cortex (PLC) and the infralimbic cortex (ILC), which have been shown to have distinct functions in the context of fear-related memory[15–17], cognitive flexibility[18] and preparatory attention and error-related events[19–23]. However, due to practical limitations related to the anatomical layout of the region, it has been challenging to study electrophysiological differences between all three subregions simultaneously with sufficient single cell data to draw meaningful conclusions about functional specializations. Some authors argue that the mPFC subregions are not distinguishable as three separate subunits, but rather function as a continuum[24]. Especially the function of the PLC is under debate, and a recent study suggested to divide the PLC further into a dorsal and ventral section, where the dorsal PLC was found to be more related to ACC firing patterns, and the ventral PLC more closely resembled the ILC[25].

The response to SWRs in the medial prefrontal cortex has been found to be specific to the place cell activity in the hippocampus during the SWR, where non-local replay events in the hippocampus are followed by a higher firing rate modulation in the medial prefrontal cortex, and this preference is predictive of future behavior[13]. The modulation to SWRs also seems to be stronger when the SWRs

occur during behavioral immobility or rest, compared to sleep SWRs[26], potentially indicating a different mechanism underlying the two states.

Cells in the mPFC that are modulated by SWRs, are more likely to be phase-locked to the hippocampal theta rhythm seen mostly while the animal is actively exploring an environment[12,13]. Ripple and theta oscillations are independent brain states, occurring primarily during rest and active exploration, respectively. Therefore it is interesting that mPFC neurons are modulated by both states, which suggests a network of prefrontal-hippocampal activity that is co-modulated during both rest and active exploration[13].

Although the spatial specificity is lower in mPFC neurons compared to the hippocampus, some papers have reported replay trajectory events to occur in the mPFC as well[27–31]. The coordination with replay events in the hippocampus remains unclear, where one study reports coordinated replay trajectory events between the hippocampus and mPFC[31], while another study found that mPFC replay occurs independently of hippocampal replay[28]. During sleep it has been found that reactivation of previous experiences in the mPFC does occur time locked to SWRs in the hippocampus, but only when a spatial rule on the maze had been learned[30], indicating that this interaction may be selective depending on the context in which it occurs. It has also been found that the mPFC engages in replay events particularly after error trials[29], which may reflect a mechanism of negative feedback during learning. Finally, cells in the mPFC that are modulated by SWRs in the hippocampus have been shown to be less tuned to space[12], and therefore perhaps this modulation of cellular activity is not necessarily (only) a reflection of spatial replay trajectories, but may reflect another non-spatial mechanism instead.

In this study, we performed high-density probe recordings across the full depth of the mPFC and in the hippocampus simultaneously while animals are performing a behavioral task of spatial navigation, to shed light on firing properties of SWR-modulated and unmodulated cells in the mPFC. We find that mPFC cells that are not modulated by hippocampal SWRs seem to be active at key time points in spatial decision making.

Results

Chronic Neuropixels probe recordings across mPFC subregions

Adult Long Evans rats were implanted with either two Neuropixels 1.0 probes (mPFC and hippocampus; N=5 animals) or a single probe (mPFC; N=1 animal; see Methods and Fig. 1a-b and Supplementary Table 1). Signals from the mPFC were classified as originating from the dorsal or ventral subregion based on the implantation depth of the electrodes and the histological verification of the probe track (see Methods and Supplementary Fig. S1). Both subregions showed ample spiking activity (for example see Fig. 1b). In five animals, data from both dorsal and ventral mPFC was obtained and in one animal only data for the dorsal mPFC was included (due to the probe implantation being too posterior; see Supplementary Fig. S1). Spikes were assigned to a cluster (putative neuron) using automated spike sorting followed by manual curation (see Methods), and up to 203 neurons were isolated from a single subregion per session (see Fig. 1d and Supplementary Table 1). For all analyses presented here, data was averaged per session, so that sessions with a high number of neurons did not skew the results. Due to the light-weight and compact design of the implant[32], animals were able to move freely on an elevated track. While we recorded neural activity, the animals performed a spatial rule switching task in which they learned 4 different rules over the course of multiple days (see Methods and Fig. 1c). Rules were based on either allocentric ("go North" or "go South") or cue-based ("go to illuminated arm" or "go to dark arm") strategies, which were to be deducted by the animals through trial and error. Each session started with a period of 20 minutes rest in a dark resting box. After this, the animal was placed by the experimenter pseudo-randomly on either the East or the West arm of the maze and it had to learn to go (1) to the North arm, (2) to the South arm, (3) to the illuminated arm (either South or North) or (4) to the non-illuminated (South or North) arm. The order of the rules was counterbalanced between animals. The illumination of the arm was always present (also during allocentric learning) and was pseudo-randomly determined for each trial. After the animal made its choice, it was picked up by the experimenter, and placed back in the dark resting box for 30-60 seconds before continuing with the next trial. The animals were trained for a maximum of 1.5 hours or 60 trials per day. At the end of the session, animals were placed back in the dark resting box for up to 60 minutes.

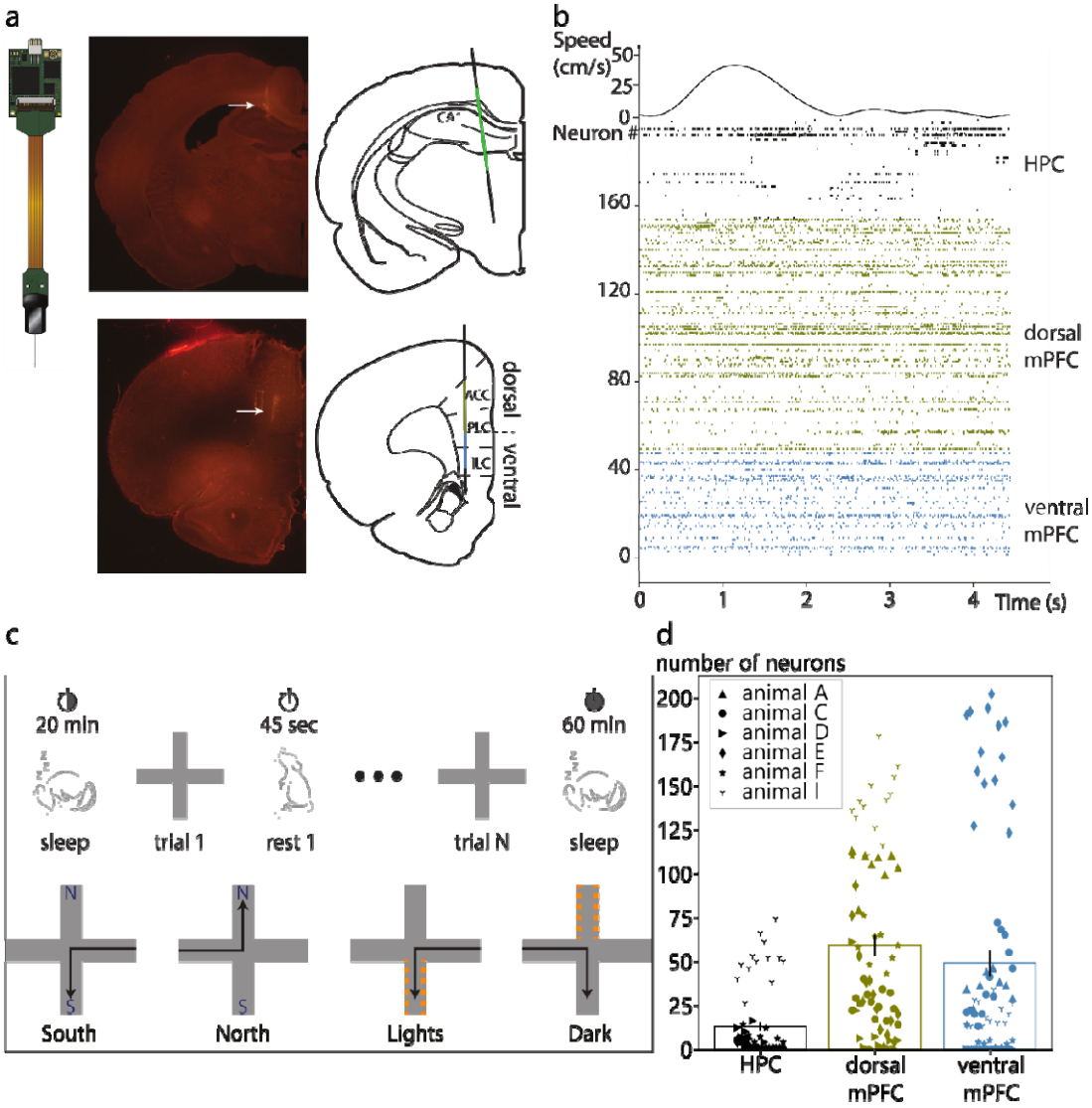

Figure 1 Chronic Neuropixels probe recordings across mPFC subregions. (a) *Left: an image of the Neuropixels probe, right: the probe mapping from one example animal where a part of the trace is seen going through the hippocampus (top) and mPFC (bottom).* ***(b)*** *An example segment of data with the animals running speed (top) and spiking activity recorded from the hippocampus, dorsal mPFC and ventral mPFC (top to bottom).* ***(c)*** *An overview of the behavioral task. Each day starts with a period of rest, followed by rule learning in the maze. Each trial is interleaved with a short period (~45 seconds) of rest, and the day ends with a period of rest or sleep of up to 60 minutes. Four different rules have to be learned over the course of multiple days, based on allocentric and cue-based strategies.* ***(d)*** *The number of sorted neurons per session for each (sub-)region. The different markers indicate different animals.*

Neurons in the dorsal and ventral mPFC are differentially modulated by hippocampal SWRs and theta phase

The mPFC is known to contain functionally distinct cell populations that differ in the modulation of their activity by hippocampal SWRs and theta oscillations[12]. Both SWR-excited and SWR-inhibited cell populations (but not SWR unmodulated cells) have been shown in the past to be phase-locked to

134 hippocampal theta oscillations and they are more likely to co-fire with cell members of their own
135 group[12]. Here we test if these cell populations are equally present across the dorsal-ventral extent of
136 the mPFC.

137 We first confirmed the presence of SWR and theta-modulated subpopulations of mPFC neurons
138 while animals were on the maze. Following hippocampal SWR onset, 13.96% of all mPFC neurons
139 significantly increased their firing rate (SWR-excited) and 5.46% of neurons decreased their firing
140 rate (SWR-inhibited). The majority of neurons were not modulated by hippocampal SWRs (80.59%;
141 SWR-unmodulated, see Fig. 2a-d). These neurons had a lower overall firing rate than SWR
142 modulated neurons (mean firing rates in Hertz, SWR-excited: M=6.25, SEM=0.49, SWR-inhibited:
143 M=9.31, SEM=1.00, SWR-unmodulated: M=3.87, SEM=0.33, ANOVA: F(142)=19.57, p<.001, see Fig.
144 2e). Cells that changed their firing rate following hippocampal SWRs also were more likely to be
145 phase-locked to the hippocampal theta oscillation. Overall, 38.46% of cells in the mPFC and 79.42%
146 of cells in the hippocampus showed significant theta phase locking, similarly to previously reported
147 percentages[33]. Theta phase-locking was more prevalent among the population of SWR-modulated
148 mPFC cells (M=55.40%, SEM=4.50) than the population of SWR-unmodulated cells (M=33.53%,
149 SEM=1.94, Mann-Whitney U test: U(104)=1993, p<.001; see Fig. 2f-g). These data are consistent with
150 the idea that SWR- and theta-modulated cells form a functional subpopulation in the mPFC.

151 Next, we tested if and how the SWR- and theta-modulated cell populations vary in the dorsal and
152 ventral subregions of the mPFC. We observed similar percentages of SWR-excited and SWR-inhibited
153 neurons in both subregions. However, the activity of SWR-excited and SWR-inhibited neurons in
154 ventral mPFC was more strongly modulated by SWRs than the activity of neurons in the dorsal mPFC
155 (mean modulation absolute z-score, dorsal: M=0.09, SEM=0.01, ventral: M=0.20, SEM=0.05;
156 independent samples t-test: t(86)=-2.11, p=.038; see Fig. 2b and Fig. 2c). The theta-modulated cells
157 were also similarly distributed in the dorsal and ventral mPFC (percent of theta modulated neurons,
158 dorsal: M=36.67%, SEM=3.07, ventral: M=42.88%, SEM=3.18; Mann-Whitney U test: U(104)=1139,
159 p=.117, see Fig. 2f). In both brain regions, there was a higher proportion of theta modulated cells
160 among the SWR-modulated compared to the SWR-unmodulated cells (percent of theta modulated
161 neurons, dorsal, SWR-modulated: M=55.53, SEM=4.85, SWR-unmodulated: M=31.93, SEM=2.51;
162 Mann-Whitney U test: U(98)=1794, p<.001. Ventral, SWR-modulated: M=59.14, SEM=5.63, SWR-
163 unmodulated: M=37.46, SEM=2.96; Mann-Whitney U test: U(88)=1354, p=.005, see Fig. 2g). The
164 preference for the hippocampal theta phase, however, was different between the dorsal and ventral
165 subregions. Phase-locked neurons in the dorsal mPFC had a bias for firing just before the peak of the
166 oscillation, while phase-locked neurons in the ventral mPFC were more likely to fire around the
167 trough of the oscillation (theta phase locking dorsal mPFC versus ventral mPFC, Kolmogorov-Smirnov

difference in distributions, SWR-modulated neurons: K=0.8, p<.001; SWR-unmodulated neurons: K=0.5, p=.012; see Fig. 2h).

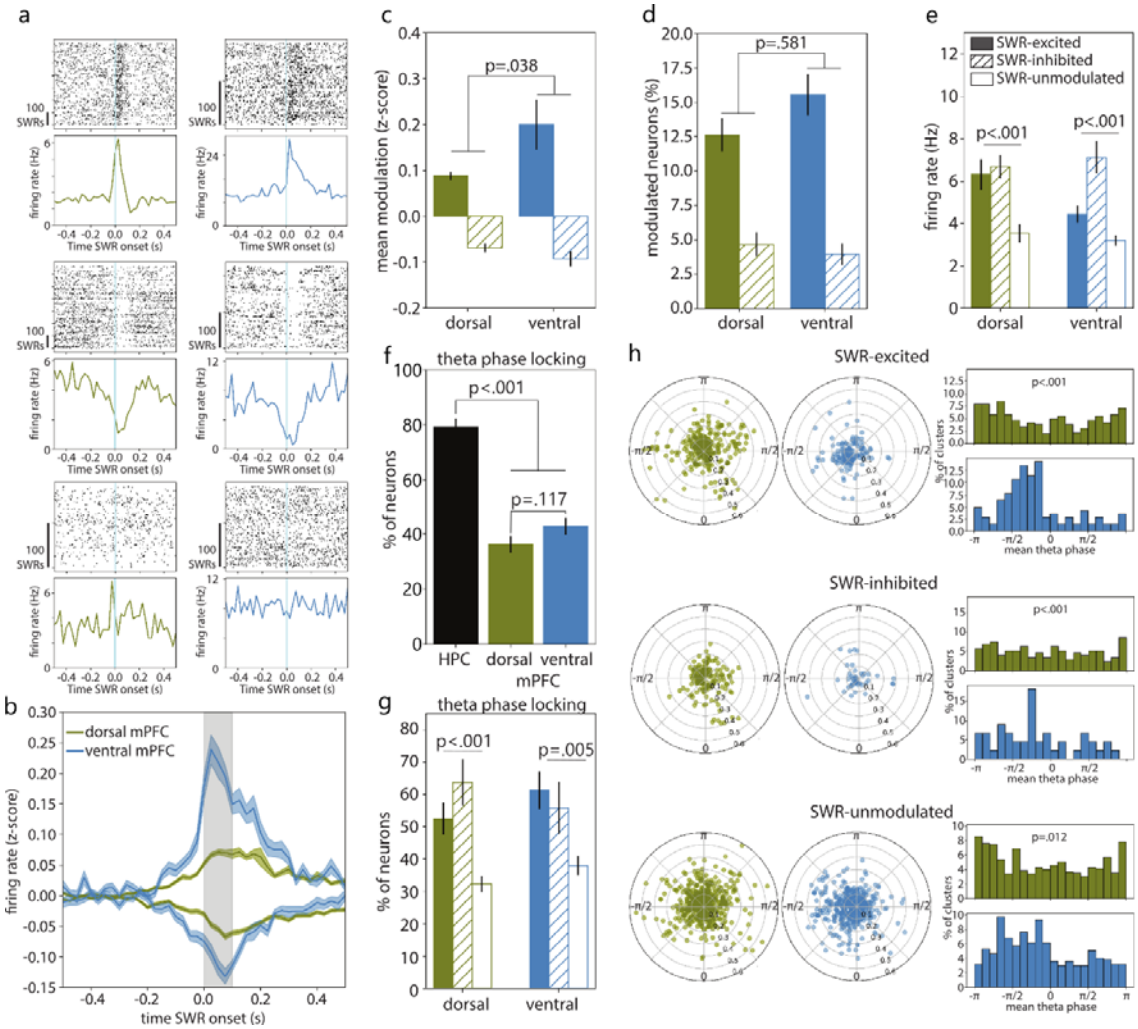

Figure 2. Neurons in the dorsal and ventral mPFC are differentially modulated by hippocampal SWRs and theta phase. *(**a**) Six example neurons in the mPFC that are SWR-excited (top), SWR-inhibited (middle) and SWR-unmodulated (bottom; dorsal mPFC in olive, ventral mPFC in blue). (**b**) The average normalized firing rates around SWR onset of all SWR-excited and SWR-inhibited neurons in the dorsal and ventral mPFC. Data is presented as mean of all neurons ± SEM. (**c**) The mean of the SWR modulation per subregion during periods of exploration in the maze. The p-value indicates the result of an independent samples t-test between the absolute modulation scores in the dorsal versus ventral mPFC. (**d**) The percentage of neurons that is SWR-excited (solid fill) and SWR-inhibited (dashed fill) per mPFC subregion. The p-value indicates the result of an independent samples t-test between the dorsal and ventral mPFC. **(e)** The mean overall firing rates per subregion of SWR-excited (solid fill), SWR-inhibited (dashed fill) and SWR-unmodulated (no fill) neurons in the maze. The p-values indicate an ANOVA between the different SWR modulation categories. (**f**) The percentage of neurons that is phase-locked to hippocampal theta per brain region. The p-values indicate the results of Mann-Whitney U test between the hippocampus and mPFC, and between the dorsal and ventral mPFC. (**g**) The percentage of neurons that is phase-locked to hippocampal theta, divided between mPFC neurons that are SWR-excited (solid fill), SWR-inhibited (dashed fill) and SWR-unmodulated (no fill). The p-values indicate an ANOVA between the different SWR modulation categories. (**h**) Left panels: the mean angle (-π to π) and (0.0 to 0.6) for all dorsal mPFC clusters that were significantly phase locked to hippocampal theta, divided between SWR-excited clusters (top), SWR-inhibited clusters (middle) and SWR-unmodulated clusters (bottom). Middle panels: the mean angle and for all phase locked clusters in the same configuration as the left panels, but for*

the ventral mPFC. Right panels: histograms of the mean angles of all theta phase-locked clusters that were SWR-excited, SWR-inhibited or SWR-unmodulated (top to bottom). The p-values indicate the result of a Kolmogorov-Smirnov test to test the difference in distribution between the dorsal (olive) and ventral (blue) mPFC.

SWR-unmodulated neurons are spatially tuned, directionally selective and show theta cycle skipping

Previous research has demonstrated that neurons in the mPFC encode spatial information[27–29,34], and suggested that SWR-unmodulated neurons show lower spatial coverage (i.e. higher spatial tuning) than SWR-excited and SWR-inhibited neurons[12]. Another paper found that the dorsal mPFC has higher spatial tuning properties than the ventral mPFC[35], from which the authors concluded that spatial tuning in the mPFC is only partly dependent on direct input from the hippocampus. Here we tested whether the difference in spatial tuning between SWR-modulated and SWR-unmodulated neurons holds up when comparing the dorsal and ventral mPFC. We calculated the spatial specificity score for each cluster (see Methods) and found a higher spatial tuning score in the hippocampus (spatial information in bits/spike, M=0.64, SEM=0.06) than in the mPFC neurons (M=0.31, SEM=0.01, Mann-Whitney U test: U(106)=2129, p<.001; Fig. 3a-b), as expected from previous literature[12,28]. In contrast to the mentioned study[35], we did not observe differences between spatial tuning properties of neurons in the dorsal and ventral mPFC (spatial information in bits/spike, dorsal: M=0.32, SEM=0.01, ventral: M=0.34, SEM=0.02; Mann-Whitney U test: U(121)=1969, p=.639). We did, however, find that SWR-unmodulated mPFC neurons showed a higher spatial tuning score (M=0.33, SEM=0.02) compared to SWR-excited (M=0.22, SEM=0.01) and SWR-inhibited neurons (M=0.11, SEM=0.01; Kruskal-Wallis: H(142)=70.52, p<.001; Fig. 3b). This effect is robust and was seen for both the dorsal and ventral subregions.

Cells that fire selectively during particular head directions have been found in a variety of brain regions as well[36–38]. We next investigated whether neurons in the mPFC are linked to certain head directions and whether there is also a differential involvement of SWR-modulated and unmodulated neurons in head direction selective firing patterns. We categorized the animals' head directions at the start of the maze in three categories (towards future choice or alternative choice, towards North or South, and towards left or right, see Methods and Fig. 3c). First, we determined for each neuron whether it spiked significantly more for one direction compared to its opposite counter part (e.g. future choice versus alternative choice). In the hippocampus 31.35% of clusters (SEM=4.20) showed significant directional selectivity, compared to 24.78% of clusters in the mPFC (SEM=1.52, Mann-Whitney U test: U(103)=1505, p=.176; chance level is 15%; see Fig. 3d). Next, for each neuron a directional selectivity index was calculated, where the difference between the firing rates within one category were subtracted from the summed firing rate of that category (e.g. the difference between firing rates during head directions towards the future choice and alternative choice, divided

225 by the sum of both direction; see Methods). This index thus indicates the preference of each neuron
226 to fire selectively during one type of head direction. For all three head direction categories (future
227 versus alternative, North versus South, and left versus right), the SWR-unmodulated neurons
228 showed significantly higher directional selectivity scores than the SWR-excited and SWR-inhibited
229 neurons (maximum absolute directional selectivity index, SWR-excited: M=0.37, SEM=0.02, SWR-
230 inhibited: M=0.27, SEM=0.02, SWR-unmodulated: M=0.48, SEM=0.02; Kruskal-Wallis: H(138)=41.26,
231 p<.001, see Fig. 3f). On a population level, there was no preference for any one of the categories
232 over another (see Supplementary Fig. S3b).

233 Furthermore, both the mPFC and hippocampus are known to encode information about
234 upcoming trajectories in alternating cycles of theta oscillations[39–41]. A subset of cells in the
235 hippocampus and mPFC are found to skip every other cycle within the theta rhythm, and neurons in
236 the mPFC are thereby thought to favor the true upcoming trajectory over alternative choices[39]. Here
237 we were interested to see whether we observe differences in theta cycle skipping properties in SWR-
238 modulated and unmodulated neurons in the dorsal and ventral mPFC. For each neuron we
239 determined whether or not it showed cycle skipping properties by looking at the probability of
240 spiking at 125 ms (one theta cycle) and 250 ms (two theta cycles) in the spike time autocorrelation
241 (see Methods and Fig. 3e). A subset of neurons in the hippocampus (M=42.03%, SEM=4.70) and in
242 the mPFC (M=25.69%, SEM=1.87) showed theta cycle skipping properties. The percentage of
243 neurons showing theta cycle skipping properties was significantly higher for SWR-unmodulated
244 neurons, compared to SWR-excited and SWR-inhibited neurons (percentage of neurons showing
245 theta cycle skipping properties, SWR-excited: M=22.72, SEM=2.01, SWR-inhibited: M=12.39,
246 SEM=3.04, SWR-unmodulated: M=28.94, SEM=1.99; Kruskal-Wallis: H(140)=31.25, p<.001, see Fig. 3f
247 and Supplementary Fig. S3c).

248 Together these results indicate that the population of SWR-unmodulated neurons seem to
249 have distinct functions in terms of spatial mapping, head direction selectivity, and cycle skipping
250 properties, with a stronger involvement compared to neurons that are either excited or inhibited by
251 hippocampal SWRs.

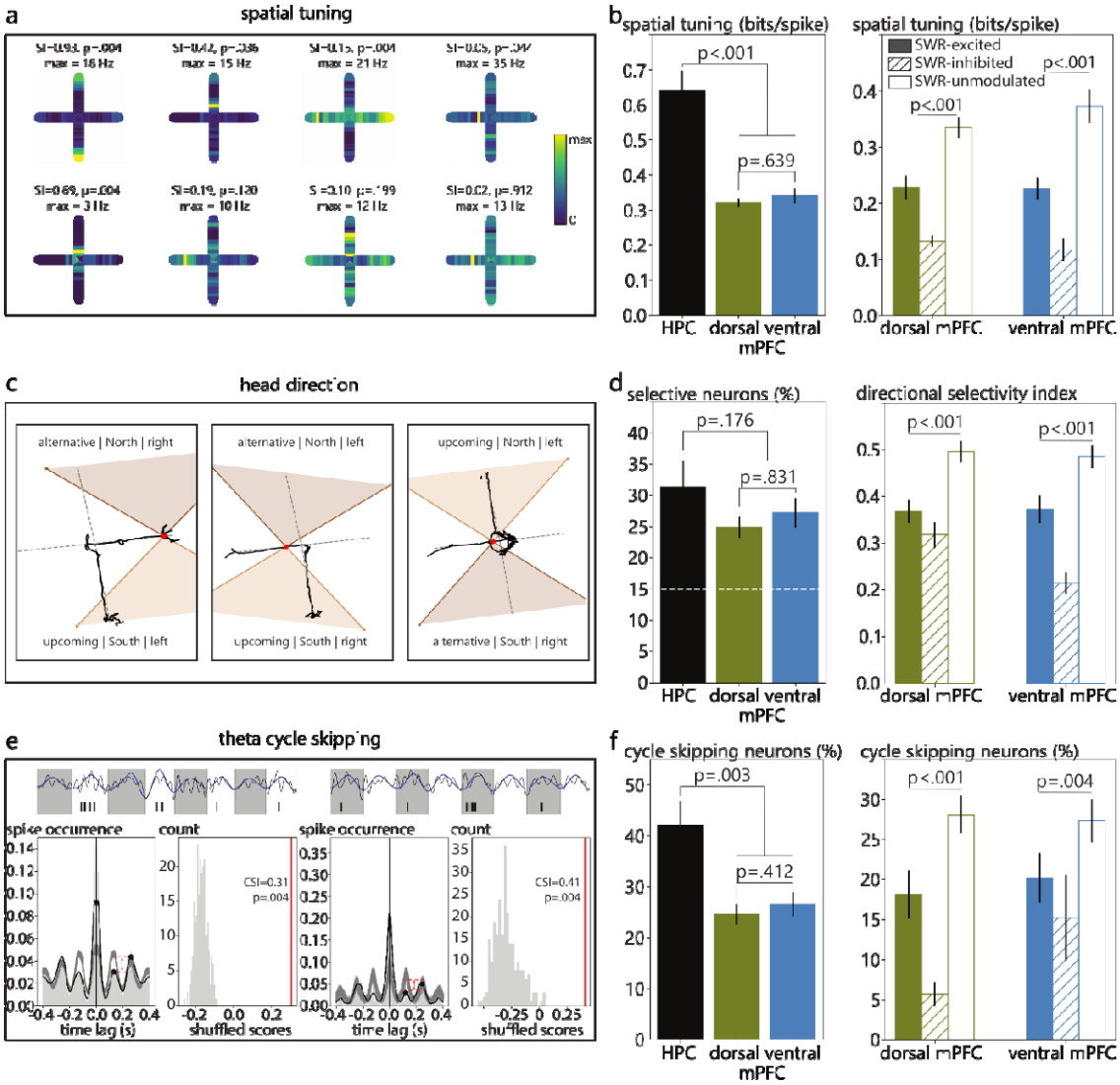

Figure 3. SWR-unmodulated neurons are spatially tuned, directionally selective and show theta cycle skipping. *(**a**) The firing patterns of eight example neurons in the maze, showing a range of spatial tuning scores (in bits/spike) sorted from highest to lowest. (**b**) Left panel: the spatial tuning score per subregion (p-values indicate a Mann-Whitney U test). Right panel: the spatial tuning score per subregion divided between mPFC neurons that are SWR-excited (solid fill), SWR-inhibited (dashed fill) and SWR-unmodulated (no fill; p-values indicate a Kruskal-Wallis test). (**c**) Three example trials where quadrants on the maze are categorized as upcoming or alternative choice, North or South, and left or right. (**d**) Left panel: the percentage of neurons that fire significantly higher than the shuffled population for at least one of the head direction categories. The chance level is indicated at 15%, as an alpha of 0.05 was maintained for each of the three direction categories (future versus alternative, North versus South, and left versus right; p-values indicate the results of a Mann-Whitney U test). Right panel: the absolute maximum directional selectivity index per subregion for mPFC neurons that are SWR-excited (solid fill), SWR-inhibited (dashed fill) and SWR-unmodulated (no fill; p-values indicate a Kruskal-Wallis test). (**e**) Spike time auto-correlations of two example neurons where the peak of the smoothed signal (in black) at 250 ms is subtracted from the peak at 125 ms and normalized to the highest of the two peaks to obtain the cycle skipping index (left panels). To determine the statistical significance, the score is compared to a shuffled population (right panels). (**f**) Left panel: the percentage of neurons that showed significant theta cycle skipping properties per subregion (p-values indicate a Mann-Whitney U test). Right panel: the theta cycle skipping index per subregion divided between mPFC neurons that are SWR-excited (solid fill), SWR-inhibited (dashed fill) and SWR-unmodulated (no fill; p-values indicate a Kruskal-Wallis test).*

Non-local representations in the mPFC are predictive of the animals' choice

Previous research has shown that the ensemble firing patterns in the mPFC can be used to decode spatial locations[29]. Furthermore, decoded position data from the mPFC has been found to contain excursions to non-local positions in the maze, which are thought to be related to the neurons' encoding of choice evaluation[29]. We were interested to see whether non-local representations in the mPFC could be linked to the future arm choice of the animals as well, and whether there is a link with hippocampal SWRs and SWR-modulated firing patterns. We decoded spatial information from spiking activity along the depth of the mPFC, using a Bayesian decoding model to associate spike features with the location in the maze at which the spikes occurred (see Methods). Using these decoding models, we were able to decode the current location of the animal based on spiking activity in the mPFC accurately (median cross-validated decoding error less than 20 cm) for a total of 40 sessions from 5 different animals. We decoded the spatial information at a theta time scale (50 ms bins with 80% overlap), and observed, aside from the local representations of the current arm, segments of representations of the other arms of the maze, that were either predictive of the upcoming choice, or of the alternative choice on the other side of the maze (see methods and Fig. 4a). Segments of non-local representations were defined as any number of consecutive time bins where the summed decoded probability of one of the two goal arms was higher than 0.5 while the animal was at the start or center of the maze (see Methods). Using the difference between the sum of decoded probabilities of the segments of the upcoming choice and the segments of the alternative choice, we obtained a prediction index between 1 and -1 corresponding to the direction the animal did and did not turn, respectively. These scores could accurately predict the turning direction of the animals, while the rule was still being learned as well as when it was already well known (see Fig. 4b).

Next, we asked if the predicted directions based on decoded non-local representations either preceded or followed the change in behavior. For this, we overlayed the learning curves of the animals with curves made from the predicted directions based on the non-local representations in the mPFC and performed cross-correlations between the two curves (see Methods and Fig. 4c). It was seen that the highest correlation between the two curves was found on average at a lag of -8 trials for the allocentric rules (M=-8.0, SEM=3.78, deviation from zero Wilcoxon one sample test: W(5)=0, p=.043) and -6 trials for the cue-based rules (M=-5.52, SEM=2.29, Wilcoxon one sample test: W(30)=96, p=.015), indicating that the decoded directions precede the real directions over the course of learning (see Fig. 4c).

306

307 Furthermore, we looked at the distribution of decoded probabilities while the animal was at
308 the choice point, but had not yet entered any of the goal arms. The distribution of decoded
309 probabilities showed an overall increase of decoded bins of the upcoming choice compared to the
310 alternative choice on the maze (interaction maze bin and prediction category, repeated measures
311 ANOVA: $F(9,351)=115.14$, $p<.001$; Fig. 4d), with most notable increases in occurrence of decoded
312 timepoints of the start (post-hoc Bonferroni corrected p-value: $p<.001$) and end (post-hoc Bonferroni
313 corrected p-value: $p<.001$) of the arm representing the upcoming choice. To look at the relative
314 contribution of SWR-modulated and unmodulated mPFC neurons, we next built separate decoding
315 models for each subpopulation (see Methods). The differences in decoded distributions between
316 the upcoming and alternative choice were also seen when using the SWR-unmodulated mPFC
317 neurons to build the decoding models (interaction maze bin and prediction category, repeated
318 measures ANOVA: $F(9,288)=30.1$, $p<.001$; post-hoc Bonferroni corrected p-values, start of the goal
319 arms: $p<.001$; end of the goal arms: $p<.001$), but not when using the SWR-modulated neurons for
320 the decoding (interaction maze bin and prediction category, repeated measures ANOVA:
321 $F(9,279)=15.53$, $p=.135$; Fig. 4d). This lack of differentiating the upcoming and alternative choices at
322 the center of the maze was true for both the SWR-inhibited and SWR-excited cell populations (SWR-
323 inhibited, interaction maze bin and prediction category, repeated measures ANOVA: $F(9,270)=27.36$,
324 $p=.193$; SWR-excited, repeated measures ANOVA: $F(9,270)=17.50$, $p=.154$). This indicates a larger
325 involvement of the SWR-unmodulated neurons in encoding the upcoming choice at the center of the
326 maze.

327 In order to compare these findings with hippocampal spatial mapping, we decoded spatial
328 activity in the hippocampus and obtained representations of upcoming and alternative choices in the
329 same way as in the mPFC (see methods and Supplementary Fig. S4). Due to more limited multi-unit
330 activity recorded from the hippocampus, we were only able to reliably decode hippocampal activity
331 from N=12 sessions from 3 different animals, but the turning direction could still be predicted
332 reliably based on the non-local representations in this region when the animals were in the process
333 of learning a spatial rule (Supplementary Fig. S4b). To look at the overlap of the decoded
334 representations between the hippocampus and the mPFC, we computed the percentage of
335 overlapping classifications for each session and compared this to shuffled data (i.e., the
336 representations in the mPFC per category of local, upcoming and alternative choices, compared to
337 N=500 times the shuffled decoded data from the hippocampus, see Methods). While the overlap
338 between the hippocampus and mPFC in local representations was significantly higher than the
339 shuffled data (overlap local representations: M=10.10% of decoded time bins, SEM=1.30, shuffled

population: M=9.08, SEM=1.13, paired samples t-test: t(10)=3.31, p=.008), no such overlap was seen for the representations of upcoming and alternative choices (overlap alternative choice: M=0.11%, SEM=0.04, shuffled population: M=0.11, SEM=0.04, paired samples t-test: t(10)=0.03, p=.973; overlap upcoming choice: M=0.48%, SEM=0.24, shuffled population: M=0.22, SEM=0.09, paired samples t-test: t(10)=1.54, p=.154; Fig. 4e). For the decoded data based on either the SWR-modulated or SWR-unmodulated neurons in the mPFC, no significant overlap in time was seen with the decoded data from the hippocampus. (Overlap local representations, SWR-modulated [shuffled]: M=7.51%, SEM=1.22 [M=6.99%, SEM=1.00], paired samples t-test: t(10)=1.28, p=.228; SWR-unmodulated [shuffled]: M=7.15%, SEM=1.04 [M=6.48%, SEM=0.82], paired samples t-test: t(10)=2.02, p=.071. Overlap alternative choice: SWR-modulated [shuffled]: M=0.92%, SEM=0.60 [M=0.29%, SEM=0.10], paired samples t-test: t(10)=1.18, p=.266; SWR-unmodulated [shuffled]: M=0.86%, SEM=0.61 [M=0.26%, SEM=0.10], paired samples t-test: t(10)=1.09, p=.302. Overlap upcoming choice: SWR-modulated [shuffled]: M=0.66%, SEM=0.19, [M=0.51%, SEM=0.11], paired samples t-test: t(10)=1.03, p=.325; SWR-unmodulated [shuffled]: M=0.80%, SEM=0.25 [M=0.51%, SEM=0.13], paired samples t-test: t(10)=1.55, p=.151. See Fig. 4e). Again, this was the case for both the SWR-excited and SWR-inhibited cell populations (Overlap upcoming choice, SWR-excited [shuffled]: M=0.25%, SEM=0.07 [M=0.18%, SEM=0.04], paired samples t-test: t(10)=1.59, p=.143; SWR-inhibited [shuffled]: M=0.86%, SEM=0.63 [M=0.27%, SEM=0.12], paired samples t-test: t(10)=1.08, p=.305. Overlap alternative choice, SWR-excited [shuffled]: M=0.61%, SEM=0.17 [M=0.46%, SEM=0.09], paired samples t-test: t(10)=1.12, p=.290; SWR-inhibited [shuffled]: M=0.33%, SEM=0.11 [M=0.29%, SEM=0.09], paired samples t-test: t(10)=0.43, p=.674). Thus, the encoding for alternative and upcoming choices on the maze is largely separated in time between the mPFC and hippocampus.

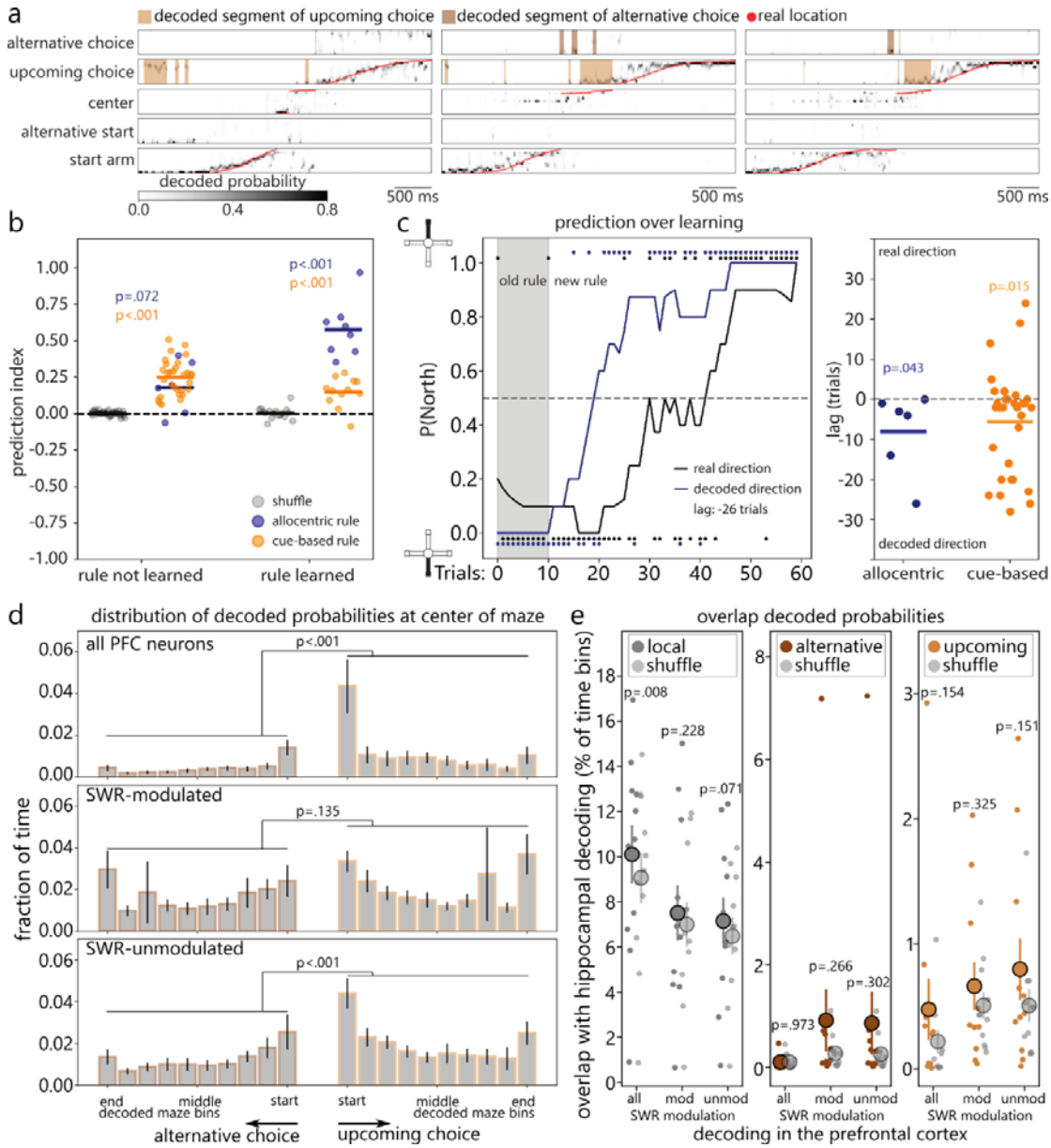

Figure 4. Non-local representations in the mPFC are predictive of the animals' upcoming choice. *(**a**) Three examples of trials where the decoded positions (grey scale) and real positions (red) are shown per maze segment. Segments of upcoming and alternative choice are highlighted with light and dark brown spans. (**b**) The prediction index per session based on the decoded non-local representations while the animal was at the start and center of the maze, separated for when the rule was not yet learned and when the rule was learned, and for the allocentric (navy) and cue-based (orange) rules. Shown in light grey is the prediction accuracy based on the shuffled decoded posteriors, and p-values indicate the result of a paired samples t-test between the real and shuffled predictions. (**c**) Left panel: an example learning curve (in black) with a rule switch from South to North after 10 trials, and the predicted directions based on the non-local representations overlayed (navy). Right panel: the lag (in number of trials) between the real direction and decoded direction per session for allocentric (navy) and cue-based (orange) strategies. A negative lag indicates that the decoded direction preceded the real direction over the course of learning. P-values indicate the result of a one-sample Wilcoxon test to test the deviation from zero. (**d**) The distribution of decoded probabilities at the center of the maze for all mPFC neurons (top panel), SWR-modulated neurons (middle panel) and SWR-unmodulated neurons (bottom panel). P-values indicate the results of a two-way repeated measures ANOVA between the maze bins and prediction categories (alternative versus upcoming choice). (**e**) The overlap between representations in the*

hippocampus and mPFC (all neurons, SWR-modulated neurons and SWR-unmodulated neurons) for the local representations (left panel), the representations of alternative choice (middle panel), and the upcoming choice (right panel). P-values indicate the results of a paired samples t-test of the percentage of overlapping decoded time bins for each session compared to the overlap of the shuffled data for that session.

Predictive representations in the mPFC are not linked to hippocampal SWRs and theta phase

Finally, we were interested to see whether the non-local representations of the upcoming choice in the mPFC are linked to hippocampal SWRs and theta phase. We obtained a histogram of SWR occurrence in temporal proximity to the start of each segment of non-local representations in the mPFC, and compared this to a shuffle distribution of decoded probabilities (see Methods). Only segments of non-local representations were included that occurred within 2 seconds of a hippocampal SWR. The occurrence of decoded segments at SWR onset were not significantly different from shuffled distributions for both upcoming and alternative choices (occurrence of segments of alternative choice at 0-20 ms from SWR onset, real: M=0.06, SEM=0.01, shuffled: M=0.07, SEM=0.01, Wilcoxon signed-rank test: W(33)=190, p=.382; occurrence of segments of upcoming choice at 0-20 ms from SWR onset, real: M=0.06, SEM=0.01, shuffled: M=0.07, SEM=0.01, Wilcoxon signed-rank test: W(33)=174, p=.147; Fig. 5a). It was further seen that the SWR-unmodulated mPFC neurons had higher normalized firing rates than SWR-modulated neurons during representations of upcoming choice (z-scored firing rates of SWR-excited neurons: M=0.24, SEM=0.07, SWR-inhibited neurons: M=0.06, SEM=0.07, SWR-unmodulated neurons: M=0.43, SEM=0.10, Kruskal-Wallis: H(94)=7.55, p=.023; Fig. 5b). During representations of the alternative choice, the difference was not significant (z-scored firing rates of SWR-excited neurons: M=0.18, SEM=0.13, SWR-inhibited neurons: M=0.14, SEM=0.08, SWR-unmodulated neurons: M=0.37, SEM=0.11, Kruskal-Wallis: H(94)=5.0, p=.082; Fig. 5b).

Similarly, we obtained a histogram of hippocampal theta phase at which each segment of non-local decoding occurred. Only segments of non-local representations that occurred within 'theta periods' were included (which were selected based on a running speed of >5cm/s and the absence of SWRs in the hippocampus; see Methods). The distribution of hippocampal theta phase at the onset of representations of upcoming and alternative choices was very homogeneous with no clear bias towards a particular phase of the theta cycle (Kolmogorov-Smirnov difference in distributions, alternative versus shuffled: K=0.25, p=.292; upcoming versus shuffled: K=0.15, p=.644; see Fig. 5c). As such, the average phase-locking scores of upcoming and alternative segments were not statistically significant compared to a randomized population (representations of alternative choice, Rayleigh's Z=0.03, randomized population M=0.01, CI=[0.00, 0.04], p=.060; representations of upcoming choice, Rayleigh's Z=0.01, randomized population M=0.01, CI=[0.00, 0.03], p=.116; Fig.

5d). These results thus indicate that the non-local representations in the mPFC are not directly linked in time to hippocampal SWRs and theta phase.

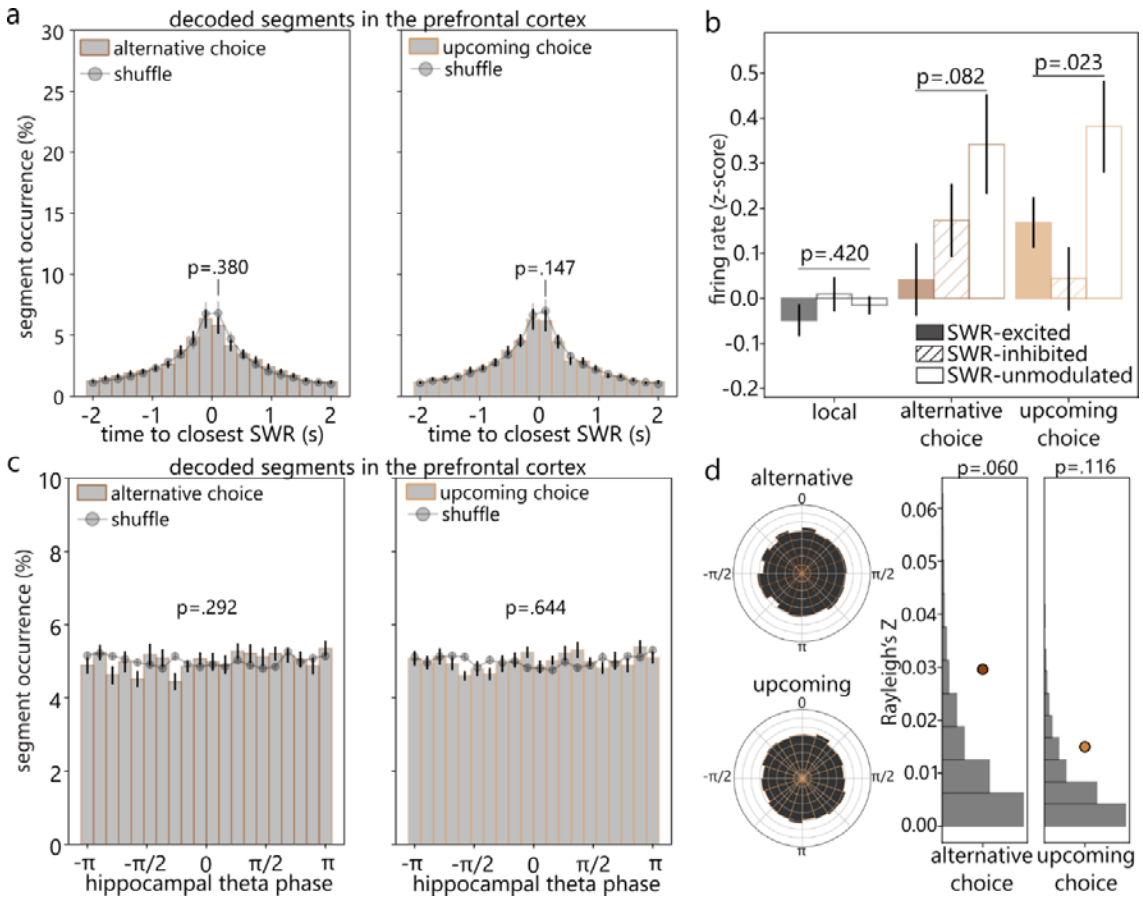

Figure 5. Non-local representations in the mPFC are not linked to hippocampal SWRs and theta phase. *(**a**) The occurrence of representations of alternative choice (left) and upcoming choice (right) in the mPFC in temporal proximity to the closest SWR. The p-values indicate the results of a Wilcoxon signed-rank test between real and shuffled data at bin 0-20 ms from SWR onset. (**b**) The firing rates of mPFC neurons that are SWR-excited, SWR-inhibited and SWR-unmodulated, during representations of upcoming and alternative choices, normalized to the average firing rate at the start of the maze. The p-values indicate the results of a Kruskal-Wallis test between the different SWR modulation categories. (**c**) A histogram of the phase of hippocampal theta oscillations at which the start of each representation of upcoming and alternative choices in the mPFC occurred. The p-values indicate the results of a Kolmogorov-Smirnov test for difference in distributions between the representations of alternative and upcoming choices compared to shuffled decoded probabilities. (**d**) Left: circular histograms of the phase locking shown in (c). Right: The phase locking score of representations of upcoming and alternative choices (Rayleigh's Z, dark and light brown dots) to hippocampal theta oscillations compared to a randomized population (gray histograms). P-values indicate the result of a left-tailed Monte Carlo test of the Rayleigh's Z compared to the shuffled population.*

432 *Predictive representations in the hippocampus are linked to SWRs and theta phase*

433 In order to compare these findings with non-local representations in the hippocampus, we obtained
434 a histogram of SWR occurrence in temporal proximity to the start of each non-local representation
435 in the hippocampus. We found that hippocampal representations of upcoming choice, but not the
436 alternative choice were more time-locked to SWRs than the shuffled probabilities (occurrence of
437 segments of alternative choice at 0-20 ms from SWR onset, real: M=0.12, SEM=0.02, shuffled:
438 M=0.12, SEM=0.01, Wilcoxon signed-rank test: W(14)=59, p=.978; occurrence of segments of
439 upcoming choice at 0-20 ms from SWR onset, real: M=0.18, SEM=0.03, shuffled: M=0.12, SEM=0.01,
440 Wilcoxon signed-rank test: W(14)=12, p=.004; Fig. 6a). Furthermore, interestingly, SWR-excited
441 neurons in the mPFC fired significantly more during hippocampal representations of upcoming
442 choice compared to representations of alternative choice (z-scored firing rates during
443 representations of alternative choice: M=-0.15, SEM=0.05, during representations of upcoming
444 choice: M=0.06, SEM=0.06, Mann-Whitney U test: U(28)=57, p=.023; Fig. 6b). For SWR-inhibited
445 neurons, the opposite effect was seen, where firing rates were higher during hippocampal
446 representations of alternative choice, and decreased during representations of upcoming choice (z-
447 scored firing rates during representations of alternative choice: M=0.15, SEM=0.10, during
448 representations of upcoming choice: M=-0.13, SEM=0.08, Mann-Whitney U test: U(28)=162, p=.042;
449 Fig. 6b). For SWR-unmodulated neurons, no difference was seen in firing rate modulation linked to
450 representations of upcoming and alternative choices in the hippocampus (z-scored firing rates
451 during representations of alternative choice: M=0.04, SEM=0.04, during representations of
452 upcoming choice: M=0.04, SEM=0.03, Mann-Whitney U test: U(28)=100, p=.619; Fig. 6b). This
453 indicates that mPFC neurons that are modulated by hippocampal SWRs, respond selectively to
454 hippocampal representations of upcoming and alternative choices.

455 Hippocampal representations of alternative and upcoming choice were differently
456 distributed with respect to the hippocampal theta cycle (Kolmogorov-Smirnov difference in
457 distributions, alternative versus shuffled: K=0.35, p=.175; upcoming versus shuffled: K=0.45, p=.034;
458 Fig. 6c). The representations of the upcoming choice occurred more during the rising phase of the
459 theta cycle (Rayleigh's Z=1.05, randomized population M=0.06, CI=[0.00, 0.23], p=.001), whereas the
460 representations of alternative choice were more scattered in relation to the hippocampal theta cycle
461 (Rayleigh's Z=0.05, randomized population M=0.09, CI=[0.00, 0.33], p=.599; Fig. 6d). Together, these
462 results indicate that while mPFC non-local representations are not time-locked to hippocampal
463 SWRs and theta phase, the non-local representations in the hippocampus are.

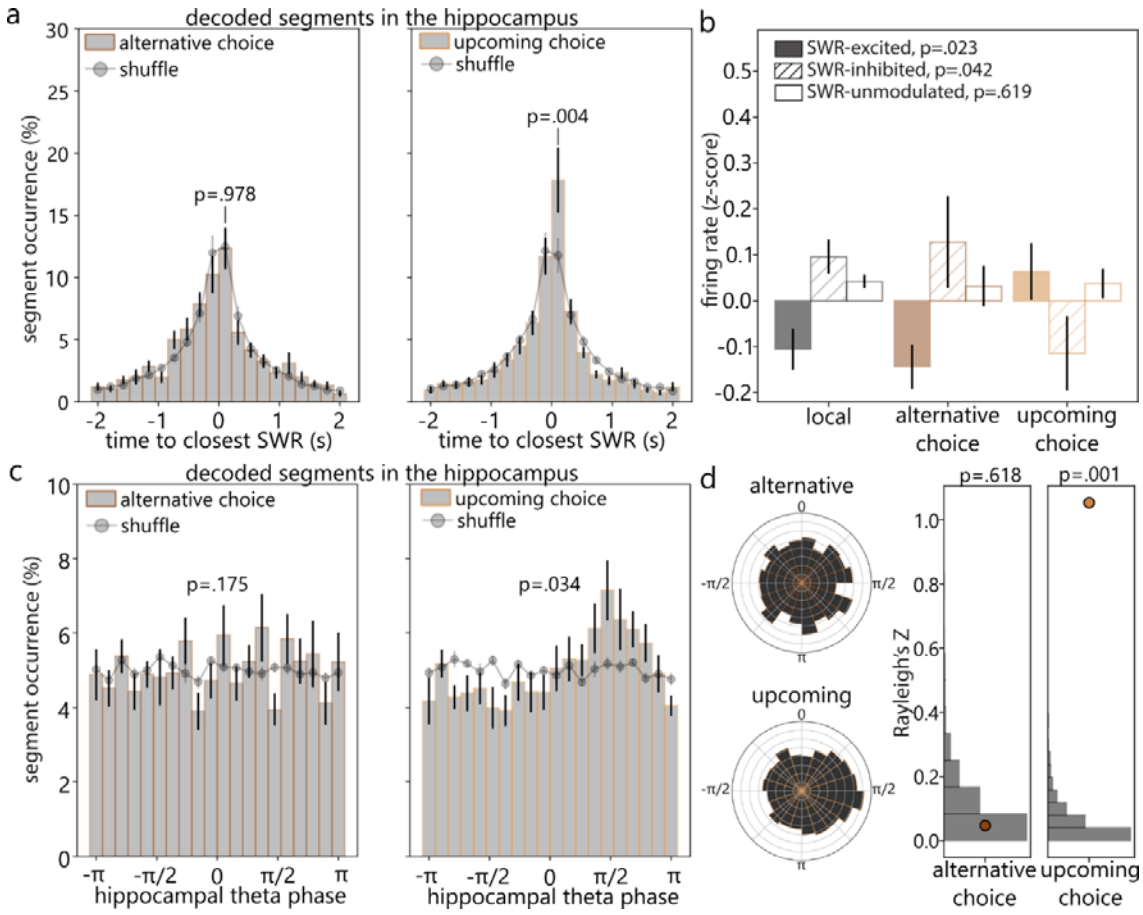

Figure 6. Non-local representations in the hippocampus are linked to SWRs and theta phase. *(**a**) The occurrence of representations of alternative choice (left) and representations of upcoming choice (right) in the hippocampus in temporal proximity to the closest SWR. The p-values indicate the results of a Wilcoxon signed-rank test between real and shuffled data at bin 0-20 ms from SWR onset. (**b**) The firing rates of mPFC neurons that are SWR-excited, SWR-inhibited and SWR-unmodulated, during representations of upcoming and alternative choices, normalized to the average firing rate at the start of the maze. The p-values indicate the results of a Mann-Whitney U test for the firing rates during upcoming and alternative representations for each of the SWR modulation categories. (**c**) A histogram of the phase of hippocampal theta oscillations at which the start of each representation of upcoming and alternative choices in the hippocampus occurred. The p-values indicate the results of a Kolmogorov-Smirnov test for difference in distributions between the representations of alternative and upcoming choices compared to shuffled decoded probabilities. (**d**) Left: circular histograms of the phase locking shown in (c). Right: The phase locking score of hippocampal representations of upcoming and alternative choices (Rayleigh's Z, dark and light brown dots) to hippocampal theta oscillations compared to a randomized population (gray histograms). P-values indicate the result of a left-tailed Monte Carlo test of the Rayleigh's Z compared to the shuffled population. Due to less multi-unit activity recorded in the hippocampus, fewer sessions were available with good decoding quality, and figure is made with N=12 sessions from 3 animals.*

484 **DISCUSSION**

485 In this study, we propose two populations of mPFC neurons that are important for spatial learning
486 and decision making. The first is more strongly influenced by hippocampal events, showing firing
487 patterns linked to hippocampal SWRs, hippocampal theta oscillations and hippocampal non-local
488 representations of upcoming choice. A second population of mPFC neurons is less modulated by
489 hippocampal events. These neurons have higher spatial tuning properties, fire more selectively
490 during certain head movements, and fire more during non-local representations in the mPFC that
491 are predictive of the upcoming choice.

492 We first showed that neurons in the mPFC are modulated by SWRs in the hippocampus, and
493 this modulation was stronger for the ventral mPFC than the dorsal section of the mPFC. The
494 hippocampus and ventral mPFC are connected through several pathways[42]. The connection with the
495 dorsal mPFC, on the other hand, is much less established. One study has reported a monosynaptic
496 prefrontal cortex projection from the ACC to the hippocampus[43], but no direct projection from the
497 hippocampus to the ACC. The denser connections with the ventral mPFC could explain the stronger
498 SWR modulation seen in the ventral compared to the dorsal mPFC.

499 Congruent to previous research[12], we next showed that mPFC neurons that were modulated
500 by hippocampal SWRs, were also phase locked to the hippocampal theta rhythm, suggesting a
501 network of hippocampal spatial mapping and mPFC firing patterns that is co-modulated during both
502 running and resting periods. We showed that these findings hold up for both the dorsal and ventral
503 mPFC, although the preferred phase of the hippocampal theta cycle was different. In the dorsal
504 mPFC, neurons fired more at the peak of the oscillation, while neurons in ventral mPFC fired more
505 just before the trough of the oscillation. An influential paper published in 2009 by Lubenov and
506 Siapas[44] has shown that theta oscillations are organized topographically across the hippocampus,
507 indicating that a segment of space, rather than a point, is represented across the hippocampus at
508 any given point in time. This concept of a 'traveling wave' of theta oscillations might translate to the
509 downstream cortical regions as well, as our data suggests that cells in the mPFC are phase locked to
510 later phases of the hippocampal theta cycle in the more ventral regions.

511 We further showed that spatial locations could be reliably decoded based on spiking activity
512 in the mPFC, and that the non-local representations at the start of the maze predicted the future
513 choice of the animal. Moreover, following a rule switch, the mPFC decoded probabilities changed a
514 few trials before the behavioral switch, which points to a leading role of the mPFC in spatial rule
515 switching. There was very little overlap between the non-local representations in the mPFC and the
516 hippocampus for the representations of the upcoming choice and alternative choices. This indicates

517 a separation in time between the two regions when engaging in the planning of future trajectories
518 and representing alternative choices.

519 Previous research has shown that spatial mapping in the hippocampus is linked to theta
520 oscillations during running[45,46], and spatial reactivations are frequently known to occur during SWRs
521 while resting[6,7,13,31,47,48]. Here we showed several pieces of evidence that suggest that spatial
522 mapping in the mPFC occurs at least partially independently from SWRs and theta phase in the
523 hippocampus. First, neurons in the mPFC that were not modulated by hippocampal SWRs, showed
524 higher spatial tuning scores, head direction selectivity and theta cycle skipping properties. The
525 spatial tuning scores and head direction selectivity indicate that these SWR-unmodulated neurons
526 are important for spatially mapping the environment, and theta cycle skipping properties in the
527 mPFC have in the past been linked to signaling upcoming choice[39,41]. The increased involvement of
528 SWR-unmodulated neurons in these functions was robust and consistent across subregions. Second,
529 non-local representations in the mPFC that were predictive of the animals' upcoming choice, were
530 not linked to hippocampal SWRs and theta phase. In contrast, non-local representations in the
531 hippocampus showed a much higher phase locking score to hippocampal theta oscillations, and
532 these predictive segments were time-locked to SWR events. Finally, SWR-unmodulated neurons in
533 the mPFC preferentially encoded the upcoming choice over the alternative choice at the center of
534 the maze, and these neurons fired more during segments of upcoming choice in the mPFC than the
535 SWR-modulated neurons. This suggests a role for signaling upcoming choice for those neurons that
536 are not modulated by hippocampal SWRs. In contrast, SWR-modulated neurons were linked to non-
537 local representations in the hippocampus, with firing rate modulations that were homologous to
538 their modulation during SWRs (SWR-excited neurons fired more during hippocampal representations
539 of upcoming choice and SWR-inhibited neurons fired less during hippocampal representations of
540 upcoming choice).

541 These findings are not directly intuitive, given the running hypothesis that that the
542 hippocampus transfers information to the cortex during SWR events[11], which could lead one to
543 hypothesize that neurons in the cortex that respond to hippocampal SWRs are responsible for
544 integrating spatial information and creating a spatial map necessary for effective spatial decision
545 making. This hypothesis is supported by several previous findings. For one, a recent paper has shown
546 that spatial maps in several cortical areas become less well defined following hippocampal lesions,
547 indicating that cortical regions rely on input from the hippocampus in order to create a spatial
548 map[49]. A recent paper from our lab further showed that disrupting the mPFC during the 200 ms
549 following SWR onset, slowed learning of a new rule in a spatial alternation task[14], indicating that the
550 input from the hippocampus during SWRs is indeed necessary for adaptive learning in response to

551 changing reward contingencies. However, none of these findings stipulate that the neurons that
552 respond to hippocampal SWRs should be the same neurons that integrate the spatial map and are
553 involved in establishing a behavioral strategy. Neurons in the mPFC that are modulated by
554 hippocampal SWRs have been shown to be selectively modulated by specific reactivation patterns or
555 replay sequences[13]. Therefore, we hypothesize that the population of neurons that is modulated by
556 SWRs is important for signaling which hippocampal reactivation patterns are important, after which
557 another population of mPFC neurons may alter its spatial map accordingly and signal the adapted
558 behavioral strategy following the external rewards and task demands.
559

560 *Suggestions for future research*

561 Together, these findings raise some interesting questions about the function of SWR-modulated and
562 SWR-unmodulated neurons in spatial learning. We hypothesize that SWR-modulated and SWR-
563 unmodulated neurons work together by respectively integrating information from the hippocampus
564 and altering the spatial map necessary for effective spatial decision making. To test this hypothesis, a
565 future study could detect SWRs in the hippocampus and inhibit mPFC activity, while also performing
566 high-density probe recordings in the mPFC to obtain information about single cell firing patterns. If
567 the SWR-linked inhibition of the mPFC alters mPFC spatial coding, by lowering the prediction index
568 of the non-local representations for example, this would support the aforementioned hypothesis.
569 Finally, subregion specific disruptions of the dorsal and ventral mPFC, using optogenetics for
570 example, could test whether there is a differential involvement of the two regions in the spatial
571 decision making process. A task with more structured time points of decision making would be
572 recommended to disentangle the times at which this information is encoded in the different
573 subregions.

574

575 *Conclusion*

576 In conclusion, neurons in the mPFC are able to predict future choice on a maze on a trial-to-trial
577 basis and their prediction precedes the behavioral change over the course of learning. This suggests
578 an important role for the mPFC in spatial learning and decision making. Our results further show that
579 SWR-unmodulated neurons are active at key time points in spatial decision making, and timepoints
580 of non-local decoding in the mPFC and hippocampus do not tend to overlap. This indicates that SWR-
581 modulation is likely not the driving factor behind the non-local decoding in the PFC.

582

METHODS

Animals

Six male Long Evans rats were used in this study, weighing between 300 and 400 grams. The animals were allowed at least one week to acclimatize upon arrival, during which time they were housed in pairs and had unlimited access to food and water. During the course of the experiment, the rats were single housed and kept at a mild food restriction schedule, maintaining over 85% of their initial body weight.

Apparatus

The experiments were conducted in a room of 2.9 by 4.2 meters, with in the center a plus shaped maze that was elevated 50 cm above the ground. The four arms of the maze were 60 cm each, with at the end a platform of 20 by 20 cm holding a reward container, and in the center a piece of 38 by 38 cm.

Pre-training

Pre-training was performed with a protocol adapted from previous literature[50], and consisted of four stages during which the animals slowly got acclimatized to the maze and learned to forage for food reward pellets (chocolate covered rice cereal). First, the rats were familiarized with the maze during 5 minutes of free exploration. Next, the day after, 10 reward pellets were spread across the maze and the animals were allowed to forage for 15 minutes. On the third day, three reward pellets were placed in each of the four reward containers and the animal was again allowed to forage for 15 minutes. After this, on all consecutive days, only one reward pellet was placed in each reward container, and the animal had to empty all four reward containers in order for them to be refilled. The maze familiarization was completed when the animal consumed all four rewards at least four times within 15 minutes. The animals took on average 8 days to complete the pre-training.

Allocentric and cue-based rule learning on the plus maze

Animals had to learn allocentric and cue-based rules in the maze, which were to be deducted through trial and error over the course of multiple days. Each day started with a rest period of 20

615 minutes. After this, the animal was placed by the experimenter on either the East or the West arm of
616 the maze pseudo-randomly and it had to learn to turn to the North, South, illuminated or non-
617 illuminated arm. The order of the rules was counterbalanced between animals, and the illumination
618 of the arm was always present (also during allocentric learning) and was pseudo-randomly
619 determined for each trial. After arriving at the end of the goal arm, the animal was picked up by the
620 experimenter and placed back in the dark resting box for 30-60 seconds before continuing with the
621 next trial. The training lasted for a maximum of 1.5 hours or 60 trials per day. At the end of the
622 session, animals were placed back in the dark resting box for up to 60 minutes. After reaching the
623 learning criterium (more than 80% of trials correct on three consecutive days), the animals
624 underwent probe implantation surgery (see below). After surgery, the same rule was reinstated until
625 learning criterium. After reinstatement, the rule was switched, either within the same strategy (i.e.,
626 rule reversal – from North to South), or to a different strategy (i.e. attentional Set-shift – from North
627 to Illuminated arm), without any indication for the animal. Throughout learning, one of two sounds
628 was played every time the animal passed a sensor halfway through the end arm (at 90 cm along the
629 track). The sounds, a high and low buzz, were associated with correct and incorrect trials. They
630 therefore provided feedback to the animals about whether a reward would be obtained, a few
631 seconds before actually receiving it. Which sound was played to indicate the outcome was
632 counterbalanced across animals but remained constant for each animal during learning. The
633 recordings were completed once the animals had learned all four rules.

634

635 *Implant preparation*

636 To record electrophysiological signals from the hippocampus and mPFC simultaneously while the
637 animals were freely moving in the maze, a dual probe implant was used, designed to hold two 1.0
638 Neuropixels probes (Imec, Leuven, Belgium) at a distance of 6.28 cm[32]. For one of the six animals,
639 there was no probe implanted in the hippocampus, so this animal was excluded from the SWR-
640 related analyses. Prior to implantation, the implant was assembled containing the two probes. The
641 probes were aligned in the stereotaxic frame to be as parallel to each other as possible and
642 perpendicular to the base of the implant. Two holes at the base of the implant were covered in a
643 mixture of bone wax and mineral oil, and the whole surface was cleaned with Baytril (50 mg/ml). The
644 probes were dipped in isopropanol for sterilization, and then in DiI (DIIC18(3) orange/red
645 carbocyanine dye 549/565 nm, VWR, Radnor, Pa, USA) for visualization of the probe tracks later on.

646

647 *Surgical procedures*

648 Surgery was performed under full anesthesia, using isoflurane (1-2%) administered via a nose cap
649 and adjusted according to the vital signs of the animal (measured with PhysioSuite monitoring
650 system, Kent Scientific, Torrington, CT, USA). A stereotaxic frame with ear bars kept the head in
651 position and the eyes were covered with eye ointment and aluminum foil for protection. After
652 shaving and disinfecting the area, a midline incision was made from the eyes to the ears, exposing
653 both the lambda and bregma on the skull. Craniotomies were drilled above the right hemisphere at
654 the coordinates 2.0 ML and -3.4 AP for the hippocampus and 0.4 ML and +2.7 AP for the mPFC. After
655 carefully removing the dura in both craniotomies, the probes were inserted with a micromanipulator
656 at a speed of 20 µm/s to a depth of maximum 7 mm.

657 The implant was anchored with 8 self-tapping bone screws (1.19 x 4.8 mm self-tapping bone screws,
658 19010-00, Fine Science Tools, Foster City, CA, USA) placed in a semi-circle in the scull around the
659 implant. One of the posterior screws was connected to grounding wire which in turn connected to
660 the ground of both probes. The implant was fixed using C&B Metabond (Parkell, Edgewood, NM,
661 USA) covering all the bone screws and the exposed part of the scull. After this, the isoflurane level
662 was lowered to 0% and the animal was carefully monitored while regaining consciousness. Post-
663 operative care included subcutaneous injections of 0.35 ml Metacam as an analgesic and topical
664 application of antibacterial cream (Picri-Baume) and an anesthetic cream (lidocaine) immediately
665 after surgery and on the three days following.

666

667 *Histology*

668 After completing all the training, animals were euthanized using pentobarbital (5ml intraperitoneal
669 injection of Dolethal, 200 mg/ml). Consecutively, they were perfused transcardially with phosphate
670 buffered saline (PBS), followed by a 4% formaldehyde solution. The brain was removed and stored in
671 a cold room (4°C). After 24 hours, it was transferred to a 30% sucrose solution where it was left for
672 at least three days, until it sank to the bottom of the tube. Brains were sectioned using a vibratome
673 (VT1000 S, Leica, Wetzlar, Germany) at 100 µm thickness, after which they were left to dry
674 overnight. Brain sections were stained with a fluorescent Nissl stain (NeuroTrace 530/615 Red
675 Fluorescent Nissl Stain, Thermo Fisher, Waltham, MA, USA), and the probe tracks were visualized
676 with a fluorescent microscope (MVX10, Olympus, Tokyo, Japan). In order to define the subregions of
677 the mPFC, the probe tracks were reconstructed and mapped using a rat brain atlas[51]. To get the
678 most accurate estimation, information was used from the histological images, together with the
679 known insertion depth during surgery, and the electrophysical signatures in the hippocampus (depth

680 at which SWRs occurred). For one animal only the dorsal mPFC was included, and for the other five
681 animals we recorded from both subregions (see Supplementary Fig. S1).

682

683 *Data acquisition*

684 Neural data was acquired at 30 kHz using a PXIe acquisition module (National Instruments, Austin,
685 TX, USA) and SpikeGLX software (https://billkarsh.github.io/SpikeGLX/) and video data was acquired
686 at 50 Hz via an overhead camera and recorded with Cheetah software (Neuralynx, Bozeman, MT,
687 USA). An Arduino Uno (Arduino, Turin, Italy) was used to send pulses at fixed intervals but varying
688 durations to the ongoing neural data and video acquisitions, to facilitate the time alignment of the
689 two streams later on (see below).

690

691 *Data analysis*

692 *Position data.* Position data was determined using DeepLabCut[52], a deep neural network algorithm
693 designed for animal behavior tracking. 1084 frames were labelled manually indicating a red and blue
694 LED at the top of the implant, and the tail base of the animal. The model was trained for 500,000
695 iterations, and the obtained position data was then smoothed, removing any spurious position
696 detections outside of the maze area and position jumps of more than 20 pixels. The positions were
697 linearized in a range from 0 to 240 cm, where positions 0-60 and 120-180 were the two start arms
698 (West and East), and positions 60-120 and 180-240 corresponded to the two goal arms (South and
699 North respectively). For decoding, the position data was binned into 5 cm bins and smoothed with a
700 Gaussian kernel (SD = 5 cm).

701

702 *Time synchronization.* A time alignment function was created for each session in order to associate
703 the neural signals with the positions in the maze at which they occurred. The time alignment was
704 based on the duration of pulses sent to both systems (neural- and position data) generated by an
705 Arduino Uno. For each timepoint in the analysis, the corresponding timestamp of the other system
706 was extrapolated using a cross-correlation of the pulse durations.

707

708 *Spike sorting*. Data was pre-processed using CatGT (https://billkarsh.github.io/SpikeGLX/#catgt) with
709 a local common average reference (CAR), using the average between rows 2 and 8 from each
710 electrode as a reference. The pre-processed data was then sorted using Kilosort 2

711 (https://github.com/MouseLand/Kilosort/releases/tag/v2.0), with a detection threshold of 5 and a
712 lower frequency limit of 150 Hz. The output for each session was manually curated using Phy2
713 (https://github.com/cortex-lab/phy), and clusters (putative single cells) were selected based on their
714 waveform, principal component features and conformity to the refractory period. After manual
715 curation, the selected clusters (N=11657) underwent an objective quality assessment using spike
716 interface[53], where only the clusters that were compliant with the neural refractory period (an inter-
717 spike-interval violation score of less than 0.1, corresponding to less than 10% of contaminating
718 spikes) were included for further analysis. This step eliminated 2798 clusters. Then, putative fast-
719 spiking interneurons were detected based on the shape of the waveform and the overall firing rate
720 of the neuron (spike half-width < 0.15 ms and firing rate > 17 Hz)[12], which eliminated an additional
721 189 clusters. Finally, clusters that showed very low spiking in the SWR modulation windows (less
722 than 50 spikes; N=2727) were also excluded from analysis, as this could lead to spurious SWR
723 modulation classifications. These procedures led to a total of 5943 remaining clusters to include for
724 analyses.

725

726 *SWR detection.* For each animal with a probe in the hippocampus (N=5), one channel was selected
727 from the top layer of dorsal CA1. This signal was filtered between 160 and 225 Hertz, and a contrast
728 frequency signal was calculated by subtracting the average power of the neighboring frequency
729 bands (100-140 Hertz and 250-400 Hertz), in order to eliminate potential spurious detections due to
730 bursts of high frequency oscillations that are not restricted to the ripple frequency range (e.g.
731 chewing artefacts). A threshold for detection was determined by taking the median amplitude of the
732 computed contrast frequency signal, plus 9 times the median absolute deviation (MAD). A low
733 threshold of the median amplitude plus 0.5 times the MAD was used for determining the start and
734 end times. SWRs were only included if they were longer than or equal to 30 milliseconds in duration.

735

736 *SWR modulation*. Spike rates from sorted neurons in the mPFC were obtained and normalized to the
737 pre-ripple window (from 1 until 0 seconds before SWR onset). For each cluster, SWR modulation was
738 calculated by averaging the spike rates over all the SWRs of that session. Neurons were considered
739 SWR-modulated if the absolute peak of the z-score in the first 200 milliseconds after SWR onset was
740 significantly higher than the shuffled population. The shuffled population was obtained by taking the
741 spike rates of the cluster around all SWRs of that session, shuffling along the time axis, and
742 calculating the peak z-score for each of the N=250 shuffles. Statistical significance was determined
743 by using a Monte-Carlo *p*-value considering an alpha of .05.

744

745 *Theta phase locking.* Theta epochs were selected based on a running speed of more than 5 cm/s and
746 the absence of SWRs in the hippocampus. The theta phase was then calculated by filtering the
747 hippocampal LFP between 9 and 12 Hertz and taking the angle of the Hilbert transformed signal. A
748 Rayleigh's Z score with associated *p*-value was calculated for each cluster and theta phase-locking
749 was determined based on the obtained *p*-value considering an alpha of .05.

750

751 *Spatial tuning.* To calculate a spatial tuning score for each sorted cluster, the maze was segmented
752 into bins of 5 cm. To avoid SWR-modulated spiking from biasing the data, spike rates during SWR
753 windows (0 to 200 ms after the onset of SWRs) were not included in this analysis. The spike rate in
754 each maze bin was calculated by taking the number of spikes recorded in that bin divided by the
755 time spent there over the course of a session. Then the spatial tuning score was calculated using a
756 method described in previous literature[54], where the normalized spike count per maze bin is
757 multiplied by the base-2 logarithm of the normalized spike rate, and the output is summed over all
758 maze bins. This gives a spatial index score expressed in bits per spike, which indicates how much
759 spatial information each spike carries. The spatial information score was only calculated for a cluster
760 if there were at least 50 spikes in the maze during the session (more than 2 times the number of
761 bins).

762

763 *Head direction selectivity.* For each position at the start of the maze, the head direction of the
764 animals was determined based on the two LEDs on top of the animals' head. Head direction angles
765 were divided in 4 equal quadrants based on the orientation of the maze. The head directions
766 towards the goal arms were then categorized in each of three categories: towards future choice or
767 alternative choice, towards North or South and towards left or right. The spike rates during each
768 head direction were calculated for each neuron, and a neuron was labeled directionally selective if
769 the firing rate was significantly higher during one of the head directions compared to its opposite
770 counterpart (e.g. significantly higher during head directions towards the upcoming choice compared
771 to the alternative choice). Statistical significance was determined by comparing the spike rates to a
772 population of 250 shuffles, where the spike rates per trial were swapped randomly. A directional
773 selectivity index was then calculated by subtracting the overall firing rate during one direction from
774 the firing rate during the other direction and dividing by the sum of both firing rates for each
775 direction category. Thus, this resulted in three scores between -1 (the neuron fired only during head

776 directions towards the alternative choice, towards the South arm, or towards right respectively) and
777 1 (the neuron fired only during head direction towards the upcoming choice, towards the North arm,
778 or towards left). Head directions in the other two quadrants (forward and backwards) were not
779 taken into account. Since the head direction selectivity was stronger in the SWR-unmodulated
780 neurons for each of the six directions (see Supplementary Fig. S3), the overall absolute directional
781 selectivity index was calculated by obtaining the absolute maximum score out of each of the three
782 categories per neuron.

783

784 *Theta cycle skipping.* To determine the theta cycle skipping properties for each cluster, spikes were
785 extracted from periods where the animals were at the start platform, arm and center of the maze.
786 For each of the four possible trajectories on the maze (East-North, East-South, West-North, West-
787 South), an autocorrelation of spike times was obtained to determine the rhythmicity of firing from
788 one spike to the next. The average histogram of spike times was smoothed, and two peaks were
789 extracted: one at around 125 ms and one at 250 ms, corresponding to one and two theta cycles of 8
790 Hz. The theta cycle skipping index was calculated by subtracting the height of the first peak from the
791 height of the second and normalizing to the maximum height of both peaks. The highest cycle
792 skipping index was selected out of the autocorrelations from the four trajectories. The obtained
793 theta cycle skipping index was then compared to a population of N=250 shuffled scores, which were
794 obtained by a shuffling procedure designed to shuffle the spike times while keeping the existing
795 periodicity of the theta cycle (125 ms) intact.

796

797 *Decoding.* To decode spatial information from the hippocampus and mPFC, spikes were detected
798 from the CatGT pre-processed data using an amplitude threshold of -50 µV on the high frequency
799 (300-6000 Hertz) filtered signal. Five features were obtained from each detected spike: depth of the
800 channel, spike amplitude, slope of the waveform, height of the positive peak and latency to the
801 positive peak. A Bayesian decoding algorithm was built, associating the spike features with the
802 position in the maze at which they occurred[55]. Periods where the running speed was less than 15
803 cm/s were excluded from the model. A median cross-validated decoding error of less than 20 cm
804 was used as an inclusion criterium, which resulted in 40 sessions from 5 different animals for the
805 mPFC decoding and 12 sessions from 3 different animals for the decoding of the data from the
806 hippocampus. For the decoding models based on only SWR-modulated or SWR-unmodulated
807 neurons, the spike times and amplitudes were selected for each neuron that was classified as SWR-
808 unmodulated or SWR-modulated (as well as SWR-excited and SWR-inhibited separately), after which

809 the decoding model was built in the same way as the mPFC decoding, for the same 40 sessions.

810

811 *Prediction index.* To predict turning directions based on decoded data, trials were decoded with a bin
812 of 50 ms and 80% overlap, such that every 130 ms was consecutively decoded, corresponding to
813 roughly one theta cycle (at 8 Hz). The decoded probabilities were summed for each maze segment
814 (the two start arms, the center and the two goal arms), and segments of local representations,
815 upcoming choice and alternative choice were obtained by grouping probabilities together in time
816 that had a summed probability of more than 0.5 per maze segment. Segments that were 50
817 milliseconds apart were joined together. The prediction index per trial was then calculated by
818 subtracting the summed probabilities of the non-taken goal arm from the summed probabilities of
819 the taken goal arm and normalizing to the total summed probabilities of both categories. In this way,
820 a score of -1 corresponds to a trial that only contains probabilities of the non-taken goal arm, and a
821 score of 1 corresponds to a trial where all the non-local probabilities are of the taken goal arm. The
822 prediction indices were separated by whether the spatial rule had or had not been learned, and
823 which spatial rule was in place at the time (allocentric or cue-based). For determining the statistical
824 significance of the prediction index, the posterior probabilities were randomized by shuffling the
825 positions in the two goal arms for each time bin in the start, arm and center of the maze. The
826 prediction index was calculated in the same way for the shuffled data as for the real posterior
827 probabilities, and statistical significance was determined by comparing the real and shuffled data.

828 *Prediction accuracy versus learning.* To determine whether the prediction accuracy per trial was
829 leading or lagging with respect to the behavior, learning curves were obtained with a moving
830 average of N=10, and overlaid with curves made from the predicted direction based on the non-local
831 representations in the mPFC. The correlation between the two curves (Pearson's r) was calculated
832 for each trial lag of -N/2 to N/2 (N denotes the total number of trials), such that a peak of
833 correlations at a negative lag indicates that the real direction is lagging behind the predicted
834 direction and a peak of correlations at a positive lag indicates that the real direction is leading the
835 predicted direction.

836

837 *Overlap decoding mPFC versus hippocampus.* To assess the overlap of decoding between the
838 hippocampus and the mPFC, each decoded time bin (of 50 ms and 80% overlap), was classified as
839 'local' (the same arm or reward platform as the animal is physically present), 'alternative choice' (the
840 arm or reward platform that the animal does not end up visiting on this trial), 'upcoming choice' (the
841 arm or reward platform that the animal will visit), or 'other' (the other start arm, the center of the
842 maze or low decoding probabilities, i.e. <0.5, for all of the categories). Then the number of

843 overlapping classifications was counted and divided by the total number of decoded time bins of the
844 session and multiplied by 100 to obtain the percentage of overlap. For each session, the
845 classifications from the hippocampus were shuffled 500 times using a rolling method over the
846 position axis. The mean overlap of the shuffled data was compared to the true overlap per session
847 using a paired samples t-test. This procedure was repeated for the decoded data from all mPFC
848 neurons, and for the SWR-unmodulated, SWR-modulated, SWR-excited and SWR-inhibited decoded
849 data separately.

850

851 *Time-locking to hippocampal SWRs and theta phase.* To determine the time locking of segments of
852 upcoming and alternative choice in the mPFC and hippocampus to hippocampal SWRs, each decoded
853 segment of alternative and upcoming choice (any number of consecutive time bins where the
854 decoded probabilities of the alternative and upcoming choice respectively were more than 0.5), was
855 assessed for its temporal proximity to hippocampal SWRs. Only non-local segments that occurred
856 within 2 seconds of a SWR were taken into account for this analysis, and only the SWR that occurred
857 closest in time to the non-local segment was included. The histogram of temporal proximity was then
858 normalized to the total number of SWRs per session, and compared to the temporal proximity of
859 shuffled posterior probabilities (randomly rolled over the position axis for each decoded time bin). To
860 determine the phase locking to hippocampal theta, theta epochs were selected as described above
861 (based on a running speed of more than 5 cm/s and the absence of SWRs in the hippocampus), and
862 the theta phase of each decoded bin was determined using a band-pass filter of 9-12 Hertz, and
863 obtaining the angle of the Hilbert transform of this signal. Then, the histogram of theta phases was
864 obtained for the segments of alternative and upcoming choice separately and normalized to the
865 number of segments included. To determine statistical significance, the histograms were compared
866 to shuffled posterior probabilities using a Kolmogorov-Smirnov test.

867 *Statistics.* All statistical tests were performed using the SciPy library for python[56]. All comparisons
868 were done on the means per session, so that sessions with a very high number of neurons in a
869 certain subregion did not skew the results for that subregion. For every comparison, the
870 assumptions of normality and heteroscedasticity were tested and non-parametric tests were chosen
871 if the assumptions were violated. The difference between firing rates of SWR-modulated and SWR-
872 unmodulated neurons was calculated using an ANOVA or Kruskall-Wallis test (non-parametric). For
873 comparisons between two groups, independent samples t-tests or Mann-Whitney U tests (non-
874 parametric) were used.

875

Acknowledgements

We thank Frederic Michon, Cagatay Aydin and Rik van Daal for their contributions in the set-up for chronic Neuropixels probes recordings in freely moving animals and Marine Guyot for her software contributions. F.K is funded by Research Foundation Flanders (FWO), Belgium under grant number G0A5422N, and grant number G077321N and KU Leuven, Belgium C1 grant C14/17/042.

Author contributions

Conceptualization, H.d.B. and F.K.; Methodology, H.d.B. and F.K.; Software, F.K.; Formal analysis, H.d.B, and F.K.; Investigation, H.d.B; Writing - Original draft, H.d.B, and F.K.; Writing - review and editing, H.d.B., and F.K.; Visualization, H.d.B. and F.K.; Supervision, F.K.; Funding Acquisition, F.K.

Competing interests

The authors declare no competing interests

Materials & Correspondence

Correspondence and request for materials can be addressed to Hanna den Bakker.

Data Availability

The data that support the findings of this study are available from the corresponding author upon reasonable request

References

1. Pfeiffer, B. E. & Foster, D. J. Hippocampal place-cell sequences depict future paths to remembered goals. *Nature* **497**, 74–79 (2013) doi: 10.1038/nature12112.

2. Pastalkova, E., Itskov, V., Amarasingham, A. & Buzsáki, G. Internally Generated Cell Assembly Sequences in the Rat Hippocampus. *Science* **321**, 1322–1327 (2008) doi: 10.1126/science.1159775.

3. Johnson, A. & Redish, A. D. Neural ensembles in CA3 transiently encode paths forward of the animal at a decision point. *J. Neurosci.* **27**, 12176–12189 (2007) doi: 10.1523/JNEUROSCI.3761-07.2007.

4. Dragoi, G. & Tonegawa, S. Preplay of future place cell sequences by hippocampal cellular assemblies. *Nature* **469**, 397–401 (2011) doi: 10.1038/nature09633.

5. Dragoi, G. & Tonegawa, S. Distinct preplay of multiple novel spatial experiences in the rat. *Proc. Natl. Acad. Sci. U. S. A.* **110**, 9100–9105 (2013) doi: 10.1073/pnas.1306031110.

6. Gillespie, A. K. *et al.* Hippocampal replay reflects specific past experiences rather than a plan for subsequent choice. *Neuron* **109**, 3149–3163 (2021) doi: 10.1016/j.neuron.2021.07.029.

7. Ambrose, R. E., Pfeiffer, B. E. & Foster, D. J. Reverse Replay of Hippocampal Place Cells Is Uniquely Modulated by Changing Reward. *Neuron* **91**, 1124–1136 (2016) doi: 10.1016/j.neuron.2016.07.047.

8. Ólafsdóttir, H. F., Carpenter, F. & Barry, C. Task Demands Predict a Dynamic Switch in the Content of Awake Hippocampal Replay. *Neuron* **96**, 925–935 (2017) doi: 10.1016/j.neuron.2017.09.035.

9. Ólafsdóttir, H. F., Bush, D. & Barry, C. The Role of Hippocampal Replay in Memory and Planning. *Curr. Biol.* **28**, 37–50 (2018) doi: 10.1016/j.cub.2017.10.073.

10. Bendor, D. & Wilson, M. A. Biasing the content of hippocampal replay during sleep. *Nat. Neurosci.* **15**, 1439–1444 (2012) doi: 10.1038/nn.3203.

11. Buzsáki, G. Hippocampal sharp wave-ripple: A cognitive biomarker for episodic memory and planning. *Hippocampus* **25**, 1073–1188 (2015) doi: 10.1002/hipo.22488.

12. Jadhav, S. P., Rothschild, G., Roumis, D. K. & Frank, L. M. Coordinated Excitation and Inhibition of Prefrontal Ensembles During Awake Hippocampal Sharp-Wave Ripple Events. *Neuron* **90**, 113–127 (2016) doi: 10.1016/j.neuron.2016.02.010.

13. Berners-Lee, A., Wu, X. & Foster, D. J. Prefrontal cortical neurons are selective for non-local hippocampal representations during replay and behavior. *J. Neurosci.* **41**, 5894–5908 (2021) doi: 10.1523/JNEUROSCI.1158-20.2021.

14. den Bakker, H., Van Dijck, M., Sun, J.-J. & Kloosterman, F. Sharp-wave ripple associated activity in the medial prefrontal cortex supports spatial rule switching. *Cell Rep.* **42**, (2023) doi: https://doi.org/10.1016/j.celrep.2023.112959.

15. León, L. A. *et al.* Behavioral effects of systemic, infralimbic and prelimbic injections of a serotonin 5-HT2A antagonist in carioca high- and low-conditioned freezing rats. *Front. Behav. Neurosci.* **11**, 1–13 (2017) doi: 10.3389/fnbeh.2017.00117.

16. Sangha, S., Robinson, P. D., Greba, Q., Davies, D. A. & Howland, J. G. Alterations in reward, fear and safety cue discrimination after inactivation of the rat prelimbic and infralimbic cortices. *Neuropsychopharmacology* **39**, 2405–2413 (2014) doi: 10.1038/npp.2014.89.

17. Sun, W., Li, X. & An, L. Distinct roles of prelimbic and infralimbic proBDNF in extinction of conditioned fear. *Neuropharmacology* **131**, 11–19 (2018) doi: 10.1016/j.neuropharm.2017.12.018.

18. Rich, E. L. & Shapiro, M. Rat prefrontal cortical neurons selectively code strategy switches. *J. Neurosci.* **29**, 7208–7219 (2009) doi: 10.1523/JNEUROSCI.6068-08.2009.

19. Holroyd, C. B. & Coles, M. G. H. The neural basis of human error processing: Reinforcement learning, dopamine, and the error-related negativity. *Psychol. Rev.* **109**, 679–709 (2002) doi: 10.1037/0033-295X.109.4.679.

20. Holroyd, C. B. & Krigolson, O. E. Reward prediction error signals associated with a modified time estimation task. *Psychophysiology* **44**, 913–917 (2007) doi: 10.1111/j.1469-8986.2007.00561.x.

21. Hyman, J. M., Holroyd, C. B. & Seamans, J. K. A Novel Neural Prediction Error Found in Anterior Cingulate Cortex Ensembles. *Neuron* **95**, 447–456 (2017) doi: 10.1016/j.neuron.2017.06.021.

22. Sambrook, T. D. & Goslin, J. A neural reward prediction error revealed by a meta-analysis of ERPs using great grand averages. *Psychol. Bull.* **144**, 213–235 (2015) doi: 10.1037/bul0000006.

23. Totah, N. K. B., Kim, Y. B., Homayoun, H. & Moghaddam, B. Anterior cingulate neurons represent errors and preparatory attention within the same behavioral sequence. *J. Neurosci.* **29**, 6418–6426 (2009) doi: 10.1523/JNEUROSCI.1142-09.2009.

24. Howland, J. G., Ito, R., Lapish, C. C. & Villaruel, F. R. The rodent medial prefrontal cortex and associated circuits in orchestrating adaptive behavior under variable demands. *Neurosci. Biobehav. Rev.* **135**, 1–12 (2022) doi: 10.1016/j.neubiorev.2022.104569.

25. Diehl, G. W. & Redish, A. D. Differential processing of decision information in subregions of rodent medial prefrontal cortex. *Elife* **12**, 1–36 (2023) doi: https://doi.org/10.7554/eLife.82833.

26. Tang, W., Shin, J. D., Frank, L. M. & Jadhav, S. P. Hippocampal-prefrontal reactivation during learning is stronger in awake compared with sleep states. *J. Neurosci.* **37**, 11789–11805 (2017) doi: 10.1523/JNEUROSCI.2291-17.2017.

27. Jiang, X. *et al.* Replay of large-scale spatio-temporal patterns from waking during subsequent NREM sleep in human cortex. *Sci. Rep.* **7**, 1–17 (2017) doi: 10.1038/s41598-017-17469-w.

28. Kaefer, K., Nardin, M., Blahna, K. & Csicsvari, J. Replay of Behavioral Sequences in the Medial Prefrontal Cortex during Rule Switching. *Neuron* **106**, 154–165 (2020) doi: 10.1016/j.neuron.2020.01.015.

29. Mashhoori, A., Hashemnia, S., McNaughton, B. L., Euston, D. R. & Gruber, A. J. Rat anterior cingulate cortex recalls features of remote reward locations after disfavoured reinforcements. *Elife* **7**, 1–18 (2018) doi: 10.7554/eLife.29793.

30. Peyrache, A., Khamassi, M., Benchenane, K., Wiener, S. I. & Battaglia, F. P. Replay of rule-learning related neural patterns in the prefrontal cortex during sleep. *Nat. Neurosci.* **12**, 919–926 (2009) doi: 10.1038/nn.2337.

31. Shin, J. D., Tang, W. & Jadhav, S. P. Dynamics of awake hippocampal-prefrontal replay for spatial learning and memory-guided decision making. *Neuron* **104**, 1110–1125 (2019) doi: 10.1016/j.neuron.2019.09.012.

32. van Daal, R. J. J. *et al.* Implantation of Neuropixels probes for chronic recording of neuronal activity in freely behaving mice and rats. *Nat. Protoc.* **16**, 3322–3347 (2021) doi: 10.1038/s41596-021-00539-9.

33. Siapas, A. G., Lubenov, E. V. & Wilson, M. A. Prefrontal phase locking to hippocampal theta oscillations. *Neuron* **46**, 141–151 (2005) doi: 10.1016/j.neuron.2005.02.028.

34. Shin, J. D., Tang, W. & Jadhav, S. P. Awake Hippocampal-Prefrontal Replay Mediates Spatial Learning and Decision Making. *SSRN Electron. J.* (2019) doi:10.2139/ssrn.3385138 doi: 10.2139/ssrn.3385138.

35. Sauer, J.-F., Folschweiller, S. & Bartos, M. Topographically organized representation of space and context in the medial prefrontal cortex. *Proc. Natl. Acad. Sci.* **119**, 1–8 (2022) doi: 10.1073/pnas.2117300119.

36. Sargolini, F. *et al.* Conjunctive Representation of Position, Direction, and Velocity in Entorhinal Cortex. *Science* **312**, 758–763 (2006) doi: 10.1126/science.1125572.

37. Jankowski, M. M. *et al.* Nucleus reuniens of the thalamus contains head direction cells. *Elife* **3**, 1–10 (2014) doi: 10.7554/eLife.03075.

38. Lozano, Y. R. *et al.* Retrosplenial and postsubicular head direction cells compared during visual landmark discrimination. *Brain Neurosci. Adv.* **1**, 1–17 (2017) doi: 10.1177/2398212817721859.

39. Robinson, J. C. & Brandon, M. P. Skipping ahead: A circuit for representing the past, present, and future. *Elife* **10**, 1–20 (2021) doi: 10.7554/eLife.68795.

40. Tang, W., Shin, J. D. & Jadhav, S. P. Multiple time-scales of decision-making in the hippocampus and prefrontal cortex. *Elife* **10**, 1–27 (2021) doi: https://doi.org/10.7554/eLife.66227.

41. Kay, K. *et al.* Constant Sub-second Cycling between Representations of Possible Futures in the Hippocampus. *Cell* **180**, 552–567 (2020) doi: 10.1016/j.cell.2020.01.014.

42. Eichenbaum, H. Prefrontal – hippocampal interactions in episodic memory. *Nat. Rev. Neurosci.* **18**, 547–558 (2017) doi: 10.1038/nrn.2017.74.

43. Rajasethupathy, P. *et al.* Projections from neocortex mediate top-down control of memory retrieval. *Nature* **526**, 653–659 (2015) doi: 10.1038/nature15389.

44. Lubenov, E. V. & Siapas, A. G. Hippocampal theta oscillations are travelling waves. *Nature* **459**, 534–539 (2009) doi: 10.1038/nature08010.

45. Zielinski, X. M. C., Shin, X. J. D. & Jadhav, X. S. P. Coherent Coding of Spatial Position Mediated by Theta Oscillations in the Hippocampus and Prefrontal Cortex. *J. Neurosci.* **39**, 4550–4565 (2019) doi: https://doi.org/10.1523/JNEUROSCI.0106-19.2019.

46. Zielinski, M. C., Tang, W. & Jadhav, S. P. The role of replay and theta sequences in mediating hippocampal-prefrontal interactions for memory and cognition. *Hippocampus* **30**, 60–72 (2020) doi: 10.1002/hipo.22821.

47. Denovellis, E. L. *et al.* Hippocampal replay of experience at real-world speeds. *Elife* **10**, 1–33 (2021) doi: 10.7554/eLife.64505.

48. Karlsson, M. P. & Frank, L. M. Awake replay of remote experiences in the hippocampus. *Nat. Neurosci.* **12**, 913–918 (2009) doi: 10.1038/nn.2344.

49. Esteves, I. M. *et al.* Spatial information encoding across multiple neocortical regions depends on an intact hippocampus. *J. Neurosci.* **41**, 307–319 (2021) doi: 10.1523/JNEUROSCI.1788-20.2020.

50. Floresco, S. B., Zhang, Y. & Enomoto, T. Neural circuits subserving behavioral flexibility and their relevance to schizophrenia. *Behav. Brain Res.* **204**, 396–409 (2009) doi: 10.1016/j.bbr.2008.12.001.

51. Paxinos, G. & Watson, C. *The Rat Brain in Stereotaxic Coordinates*. (Academic Press, 2006).

52. Mathis, A. *et al.* DeepLabCut: markerless pose estimation of user-defined body parts with deep learning. *Nat. Neurosci.* **21**, (2018) doi: 10.1038/s41593-018-0209-y.

53. Buccino, A. P. *et al.* SpikeInterface, a unified framework for spike sorting. *Elife* 1–24 (2020).

54. Skaggs, W. E., McNaughton, B., Gothard, K. M. & Markus, E. J. An information-theoretic approach to deciphering the hippocampal code. *Neural Inf. Process. Syst.* **5**, 1030–1038 (1993).

55. Kloosterman, F., Layton, S. P., Chen, Z. & Wilson, M. A. Bayesian decoding using unsorted spikes in the rat hippocampus. *J. Neurophysiol.* **111**, 217–227 (2014) doi: 10.1152/jn.01046.2012.

56. Virtanen, P. *et al.* SciPy 1.0: fundamental algorithms for scientific computing in Python. *Nat. Methods* **17**, (2020) doi: 10.1038/s41592-019-0686-2.

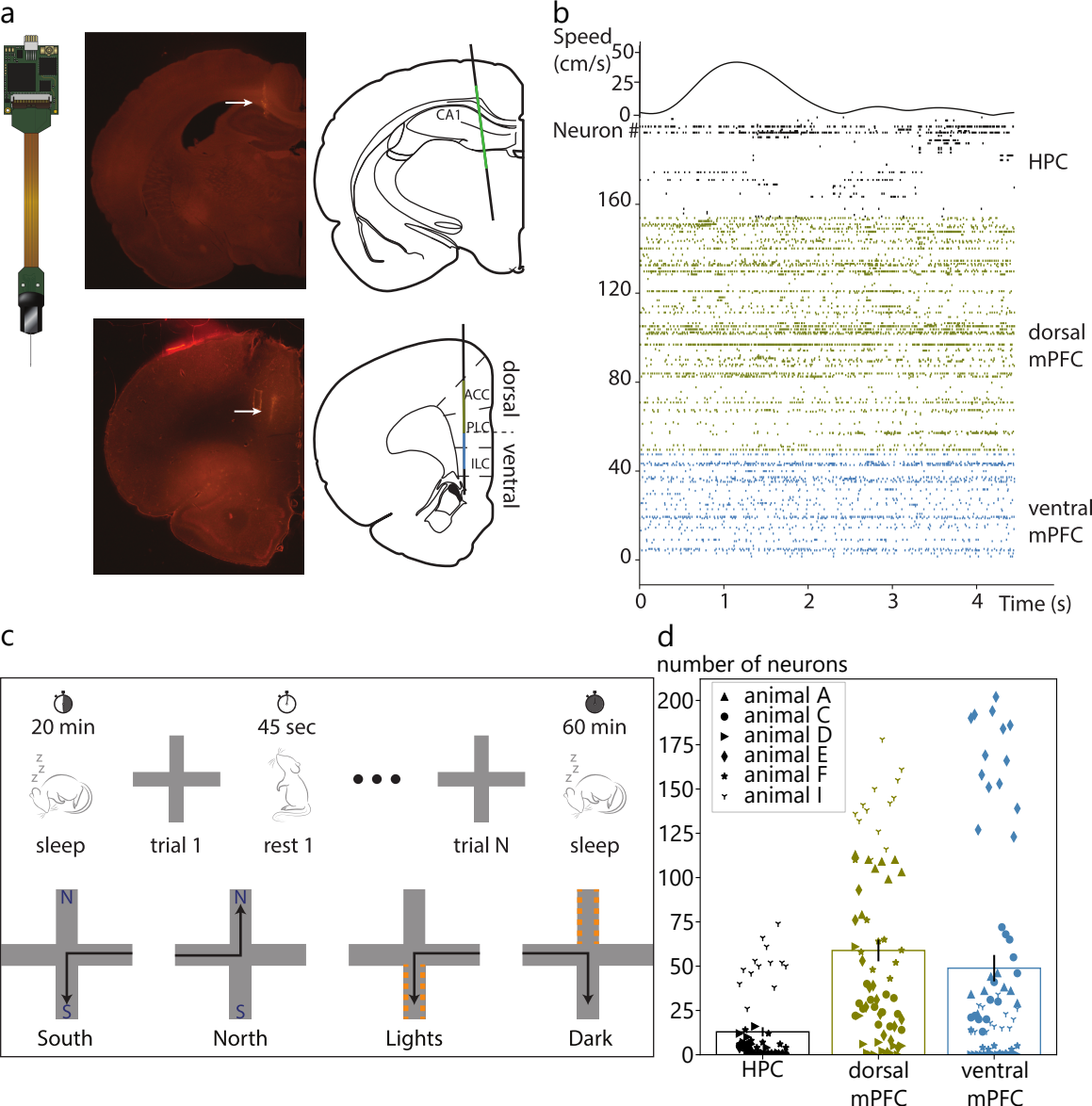
a
CA1
ACC
PLC
ILC
dorsal
ventral
b
Speed (cm/s)
50
25
0
Neuron #
160
120
80
40
0
HPC
dorsal mPFC
ventral mPFC
0
1
2
3
4
Time (s)
c
20 min
45 sec
60 min
sleep
trial 1
rest 1
trial N
sleep
N
S
South
North
Lights
Dark
d
number of neurons
animal A
animal C
animal D
animal E
animal F
animal I
200
175
150
125
100
75
50
25
0
HPC
dorsal mPFC
ventral mPFC

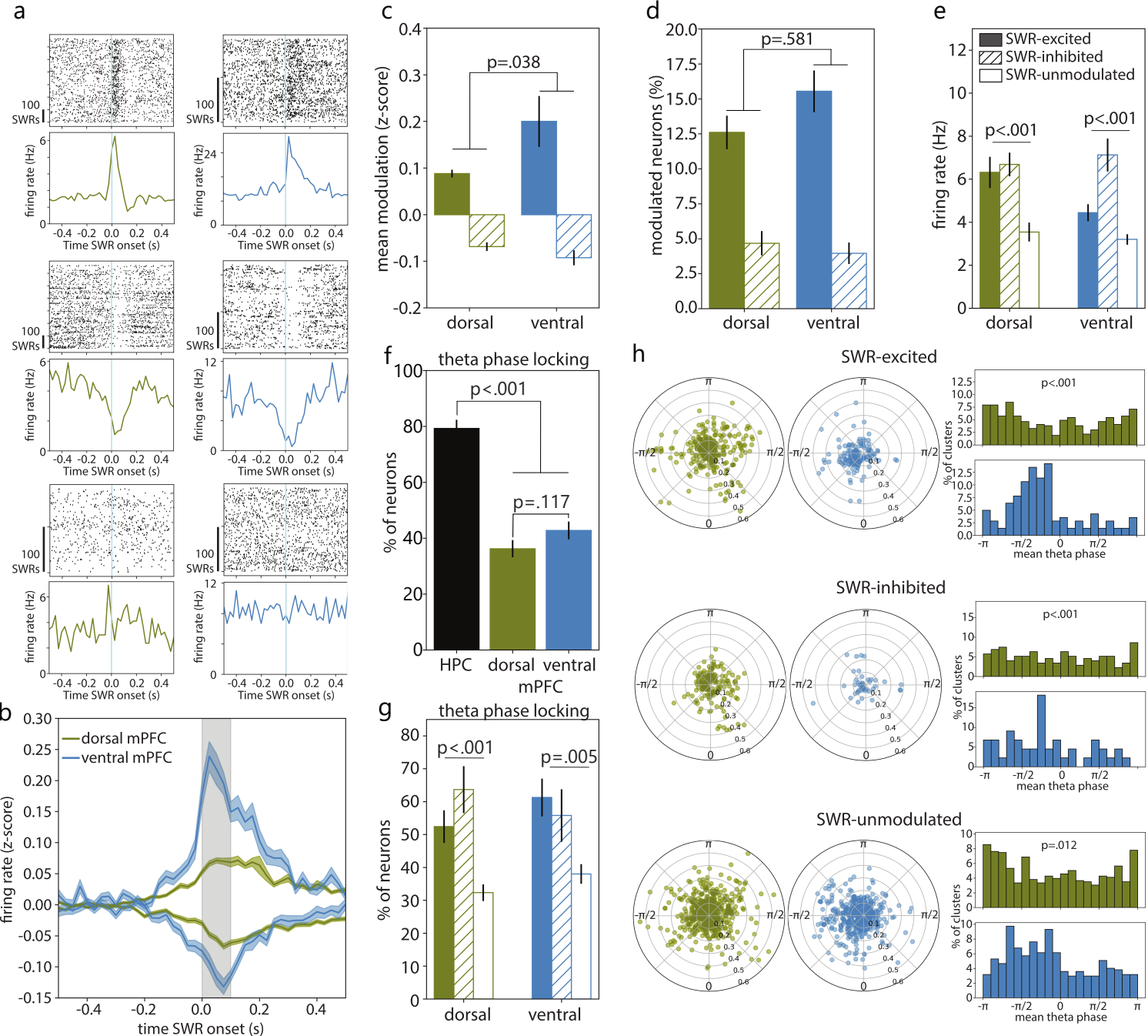
a
100 SWRs
firing rate (Hz)
Time SWR onset (s)
b
dorsal mPFC
ventral mPFC
firing rate (z-score)
time SWR onset (s)
c
p=.038
mean modulation (z-score)
dorsal
ventral
d
p=.581
modulated neurons (%)
dorsal
ventral
e
SWR-excited
SWR-inhibited
SWR-unmodulated
p<.001
p<.001
firing rate (Hz)
dorsal
ventral
f
theta phase locking
p<.001
p=.117
% of neurons
HPC
dorsal mPFC
ventral mPFC
g
theta phase locking
p<.001
p=.005
% of neurons
dorsal
ventral
h
SWR-excited
p<.001
% of clusters
mean theta phase
SWR-inhibited
p<.001
% of clusters
mean theta phase
SWR-unmodulated
p=.012
% of clusters
mean theta phase

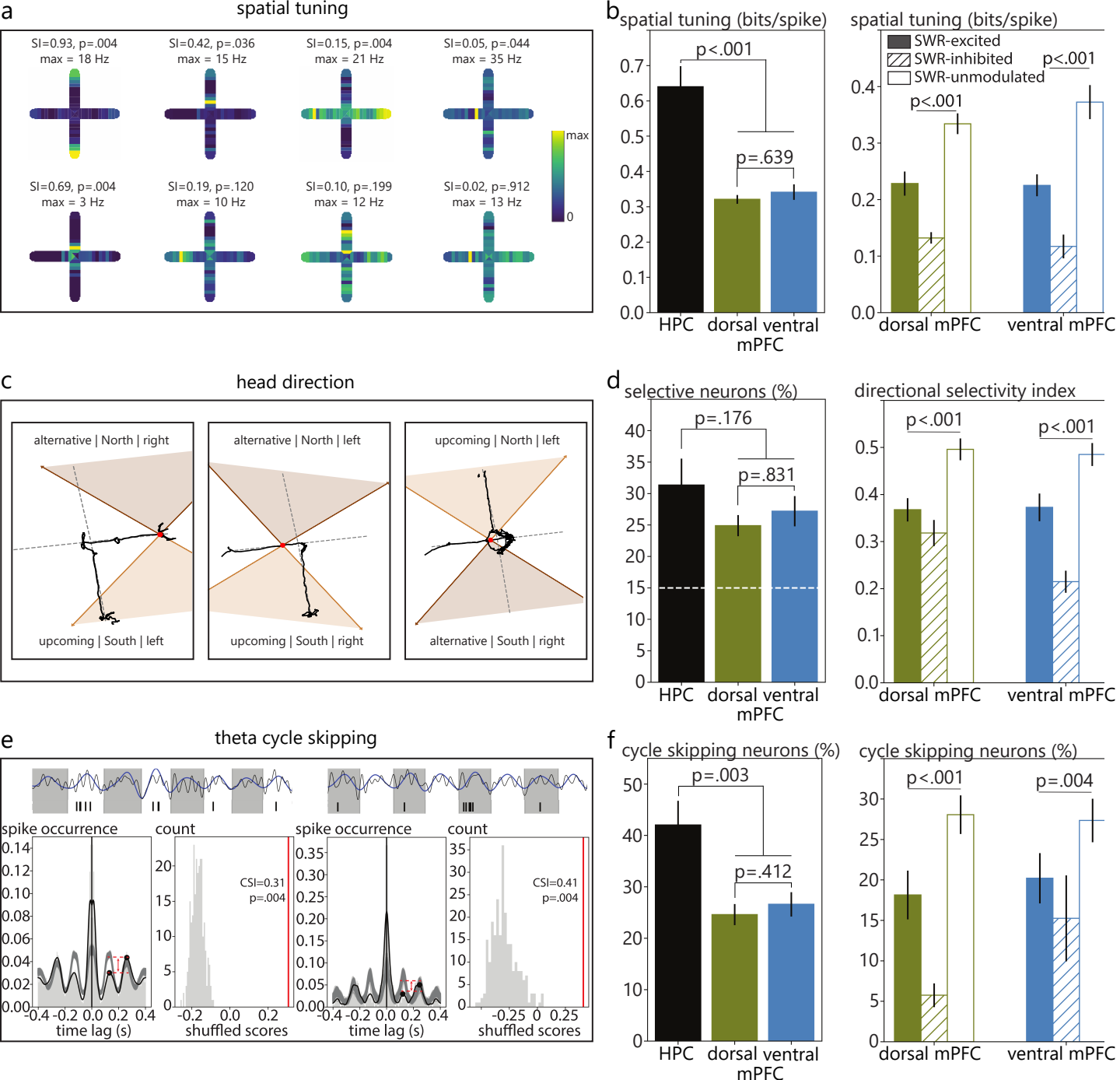
a
spatial tuning
SI=0.93, p=.004
max = 18 Hz
SI=0.42, p=.036
max = 15 Hz
SI=0.15, p=.004
max = 21 Hz
SI=0.05, p=.044
max = 35 Hz
SI=0.69, p=.004
max = 3 Hz
SI=0.19, p=.120
max = 10 Hz
SI=0.10, p=.199
max = 12 Hz
SI=0.02, p=.912
max = 13 Hz
max
0
b
spatial tuning (bits/spike)
p<.001
p=.639
HPC
dorsal mPFC
ventral mPFC
spatial tuning (bits/spike)
SWR-excited
SWR-inhibited
SWR-unmodulated
p<.001
p<.001
dorsal mPFC
ventral mPFC
c
head direction
alternative | North | right
upcoming | South | left
alternative | North | left
upcoming | South | right
upcoming | North | left
alternative | South | right
d
selective neurons (%)
p=.176
p=.831
HPC
dorsal mPFC
ventral mPFC
directional selectivity index
p<.001
p<.001
dorsal mPFC
ventral mPFC
e
theta cycle skipping
spike occurrence
count
time lag (s)
shuffled scores
CSI=0.31
p=.004
CSI=0.41
p=.004
f
cycle skipping neurons (%)
p=.003
p=.412
HPC
dorsal mPFC
ventral mPFC
cycle skipping neurons (%)
p<.001
p=.004
dorsal mPFC
ventral mPFC

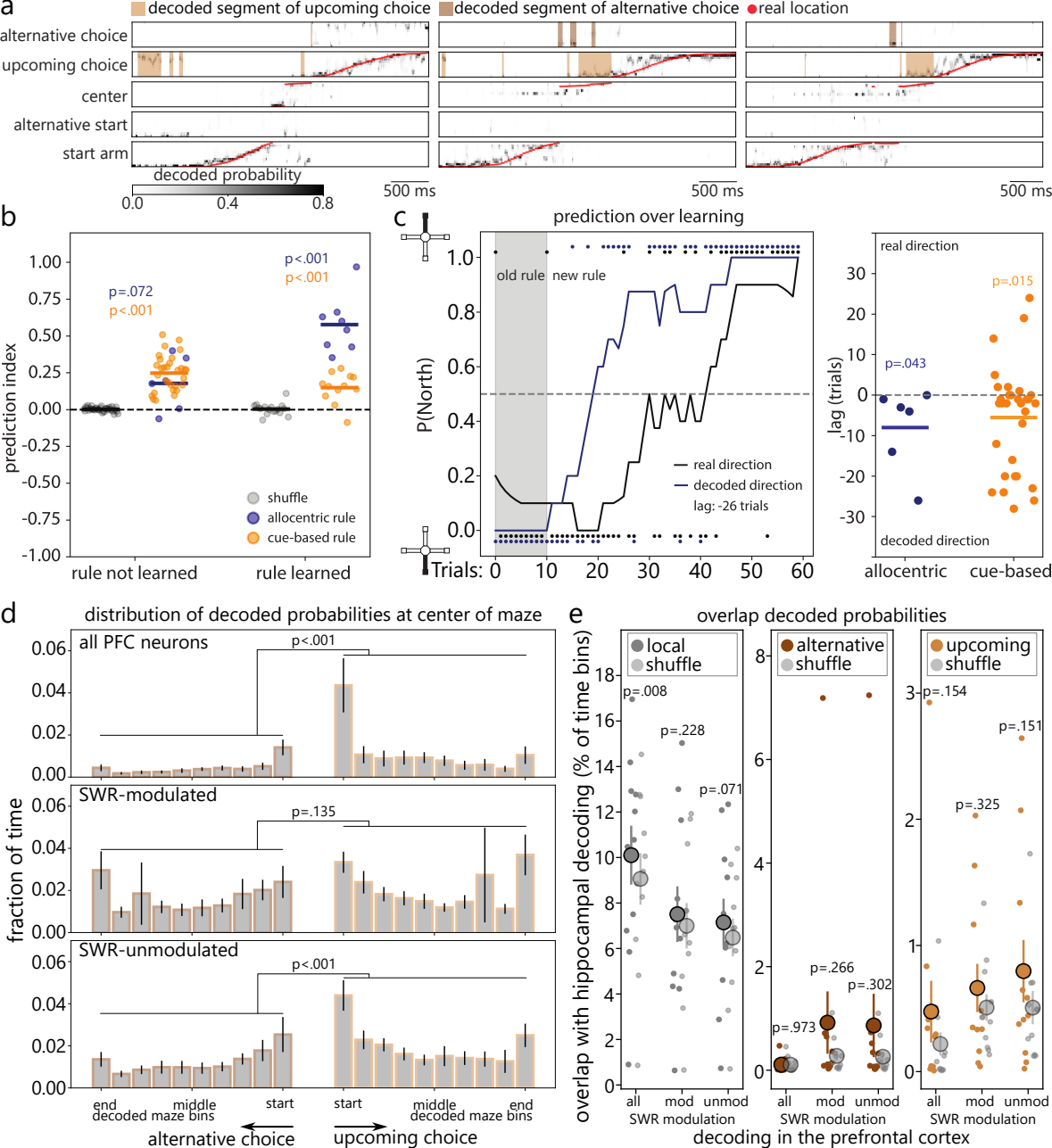
a
decoded segment of upcoming choice
decoded segment of alternative choice
real location
alternative choice
upcoming choice
center
alternative start
start arm
decoded probability
0.0
0.4
0.8
500 ms
500 ms
500 ms
b
prediction index
p=.072
p<.001
p<.001
p<.001
shuffle
allocentric rule
cue-based rule
rule not learned
rule learned
c
prediction over learning
old rule
new rule
P(North)
real direction
decoded direction
lag: -26 trials
Trials:
real direction
decoded direction
lag (trials)
p=.015
p=.043
allocentric
cue-based
d
distribution of decoded probabilities at center of maze
all PFC neurons
SWR-modulated
SWR-unmodulated
fraction of time
p<.001
p=.135
p<.001
end
middle
start
decoded maze bins
alternative choice
upcoming choice
e
overlap decoded probabilities
local
shuffle
alternative
shuffle
upcoming
shuffle
overlap with hippocampal decoding (% of time bins)
p=.008
p=.228
p=.071
p=.973
p=.266
p=.302
p=.154
p=.151
p=.325
all
mod
unmod
SWR modulation
decoding in the prefrontal cortex

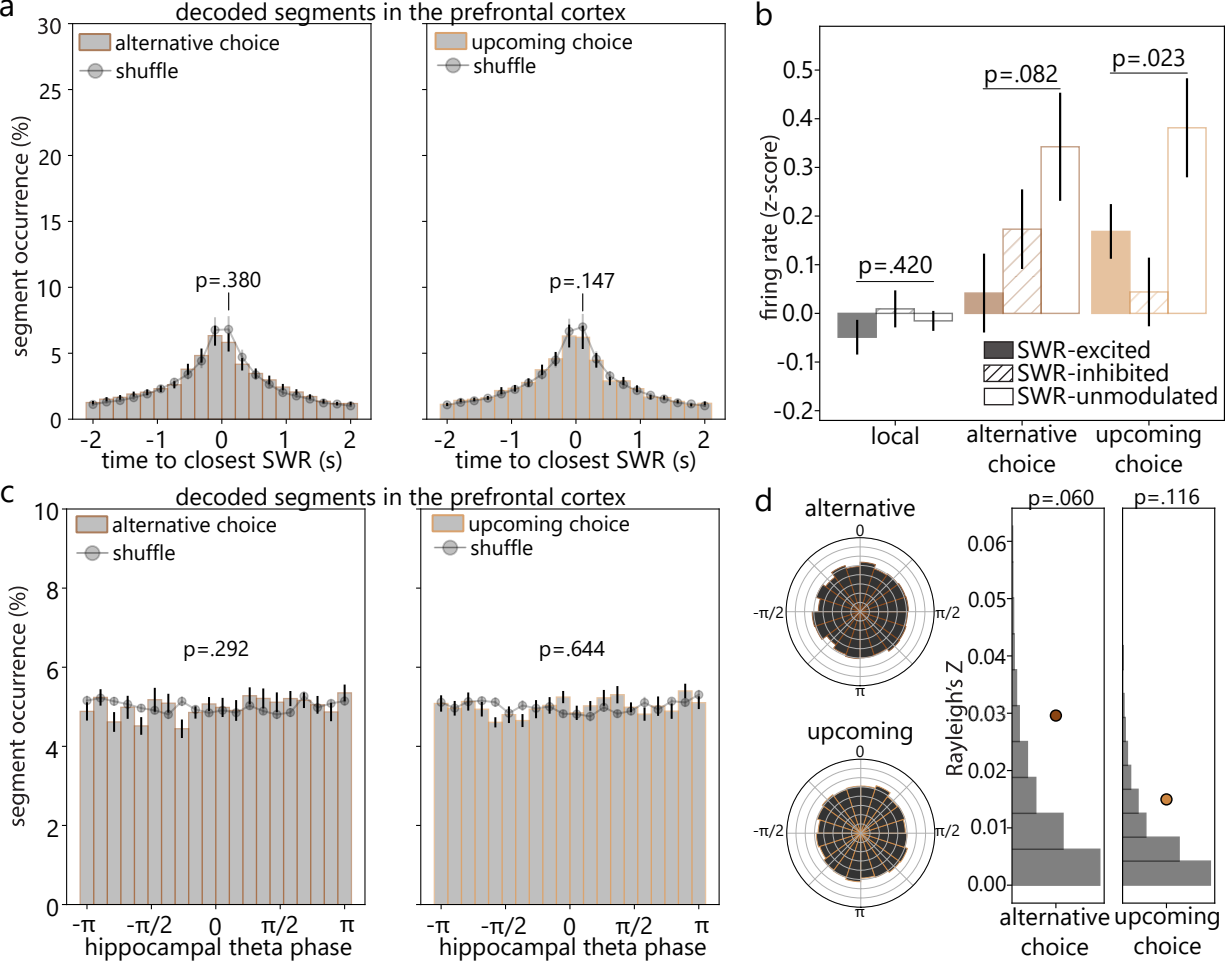
a
decoded segments in the prefrontal cortex
alternative choice
shuffle
upcoming choice
shuffle
segment occurrence (%)
p=.380
p=.147
time to closest SWR (s)
time to closest SWR (s)
b
firing rate (z-score)
p=.420
p=.082
p=.023
SWR-excited
SWR-inhibited
SWR-unmodulated
local
alternative choice
upcoming choice
c
decoded segments in the prefrontal cortex
alternative choice
shuffle
upcoming choice
shuffle
segment occurrence (%)
p=.292
p=.644
hippocampal theta phase
hippocampal theta phase
d
alternative
upcoming
Rayleigh's Z
p=.060
p=.116
alternative choice
upcoming choice

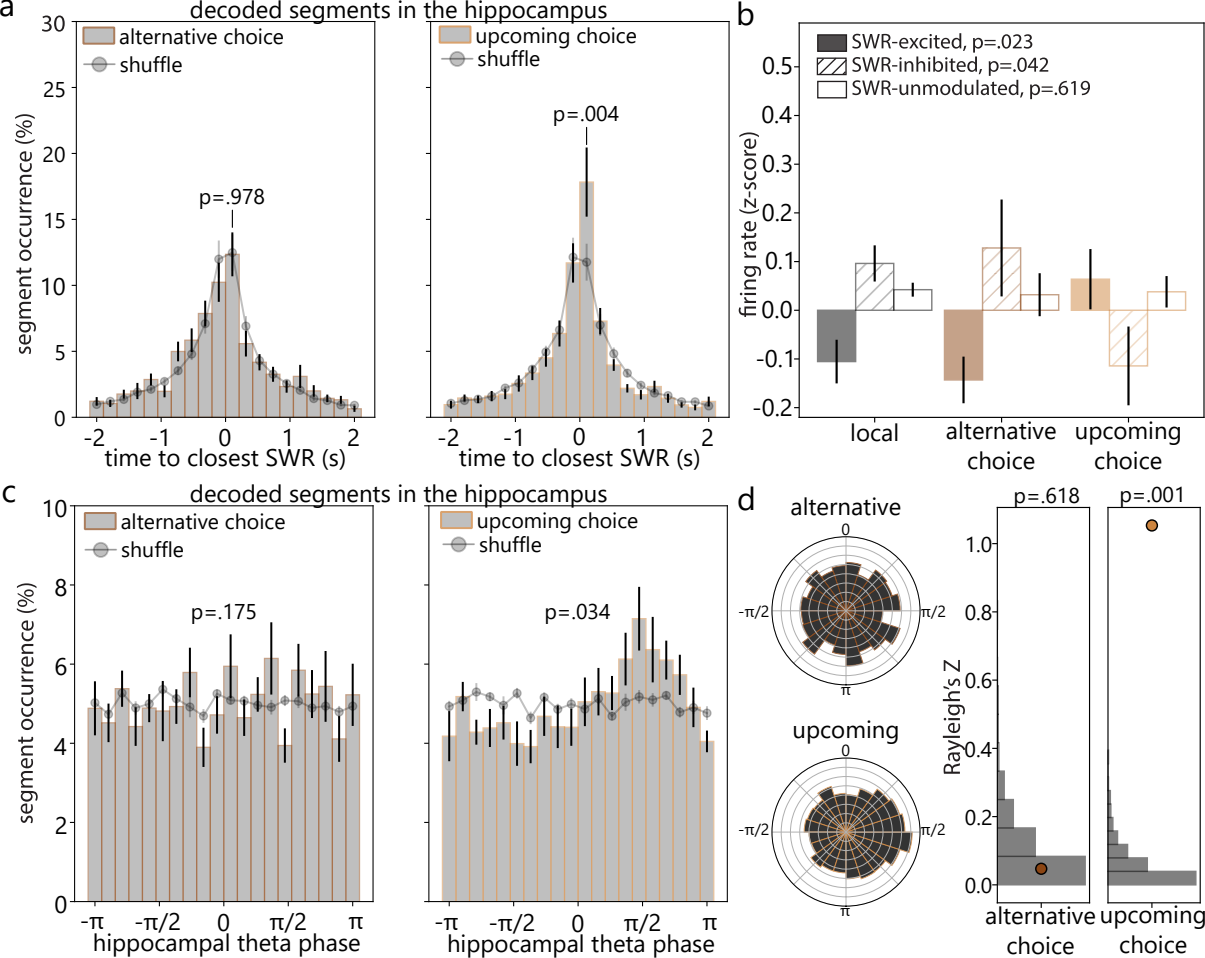
a
decoded segments in the hippocampus
alternative choice
shuffle
upcoming choice
shuffle
p=.978
p=.004
segment occurrence (%)
time to closest SWR (s)
time to closest SWR (s)
b
SWR-excited, p=.023
SWR-inhibited, p=.042
SWR-unmodulated, p=.619
firing rate (z-score)
local
alternative choice
upcoming choice
c
decoded segments in the hippocampus
alternative choice
shuffle
upcoming choice
shuffle
p=.175
p=.034
segment occurrence (%)
hippocampal theta phase
hippocampal theta phase
d
alternative
upcoming
p=.618
p=.001
Rayleigh's Z
alternative choice
upcoming choice